Evaluation of the LandscapeDNDC model for drained peatland forest managements, LDNDC v1.35.2 (revision 11434)

Ahmed Hasan Shahriyer[1], David Kraus[2], Tiina Markkanen[1], Mika Korkiakoski[1], Helena Rautakoski[1], Suvi Orttenvuori[1], Yao Gao[3], Henri Kajasilta[1], Rüdiger Grote[2], Annalea Lohila[1,4], and Tuula Aalto[1]

[1]Climate System Research, Finnish Meteorological Institute, Helsinki, Finland
[2]Institute of Meteorology and Climate Research Atmospheric Environmental Research (IMKIFU), Karlsruhe Institute of Technology, Garmisch-Partenkirchen, Germany
[3]Department of Civil Engineering, University of Hongkong, Hongkong, China
[4]Institute for Atmospheric and Earth System Research/Physics (INAR), Faculty of Science, P.O. Box 68, 00014 University of Helsinki, Helsinki, Finland

Correspondence: Ahmed Hasan Shahriyer (ahmed.hasan.shahriyer@fmi.fi)

Abstract. Rotational forestry (RF) is the prevailing management practice on drained peatlands in Finland, while continuous cover forestry (CCF) is increasingly studied for its potential climate benefits. We applied the process-based LandscapeDNDC model, for the first time, to simulate experimental peatland forest stands under three different managements: RF, CCF and non-managed ~~control~~Control. Mixed-species stands of pine, spruce, and birch were initialized, with management, partial harvest of pine in CCF and clear-cut harvest of all species in RF, leading to species shifts toward spruce–birch dominance in CCF and birch seedlings in RF. The primary objective of this study was to evaluate the performance of LandscapeDNDC model in forested drained peatlands. To this aim, we quantified the differences in gas exchange and water balance originating from differences in species composition and management methods. We also implemented modification to dynamic water table (WT) calculations and improved humus pool partitioning based on soil carbon-to-nitrogen ratios. Model evaluation against field data showed strong agreement for daily net ecosystem exchange (correlation 0.84–0.88; Nash–Sutcliffe efficiency 0.66–0.75). Modeled leaf area index (LAI) closely matched site estimates before management and Sentinel-2 satellite estimated LAI afterwards. Soil moisture and WT dynamics were realistically reproduced. Methane flux patterns were accurately captured in the control and CCF stands. Moreover, the methane flux was found to be sensitive to the WT after clear-cut in the RF stand. Modeled annual carbon balances were consistent with measurements and indicated that CCF became a carbon sink more rapidly than RF. These results demonstrate that LandscapeDNDC can reliably simulate the biogeochemical and hydrological consequences of alternative peatland forest management scenarios. The model therefore provides a valuable tool for developing climate-smart management strategies on drained peat soils.

1 Introduction

Peatlands cover 3% of the land area on Earth (Clarke and Rieley, 2019). The amount of carbon stored in northern peatlands is estimated to be around 1016–1105 Gt (Nichols and Peteet, 2019). Peatlands are often drained for use in forestry, agriculture, and peat extraction (Clarke and Rieley, 2019). In Finland, peatland drainage began in the 1920s and increased significantly in the 1960s. The drainage of peatlands expands the land area available for forestry, facilitating tree growth in regions that were previously unsuitable for productive forest development. However, draining peatlands leads to increased aeration and degradation of the peat, which increases carbon dioxide (CO_2) emissions from the soil due to increased peat decomposition (Findlay, 2021). Forests on drained peatlands make up 25% (5.7 Mha) of the total forested land area in Finland (Turunen and Valpola, 2020).

~~Soils on drained, nutrient-rich sites tend to be sources of CO_2. Emissions from peat soil are often offset by carbon fixation by the forest, at least on nutrient-poor sites (Ojanen et al., 2013)~~Forest ecosystems on nutrient rich soils have been significant CO_2 source (Ojanen et al., 2013; Lohila et al., 2007) to a small sink (Korkiakoski et al., 2023). Forest ecosystems on nutrient poor soils on the other hand have been moderate sink (Tong et al., 2024) to high sink (Laine et al., 1996; Lohila et al., 2011; Minkkinen et al., 20 . However, it may take decades for ~~the forest to reach~~ forest ecosystems to reach a net CO_2 sink after drainage, if it is reached at all ~~. Drained fen-type peatlands contain nutrient-rich peat soils compared to nutrient-poor bog-type peatlands. The carbon-to-nitrogen~~ (Quesada et al., 2026). Carbon-to-nitrogen ratio (C:N) is an often-used indicator for the nutrient status of peat soil and it is typically lower in drained ~~fens indicating nutrient-richness. The decomposition~~ nutrient rich peat. Decomposition of peat releases nutrients available to plants, and this nutrient input decreases from rich to poorer sites (Baylay et al., 2005) . Peat soils on drained nutrient-rich sites tend to be sources of CO_2 (He et al., 2016; Kasimir et al., 2018), while in nutrient-poor sites may act as a carbon sink (Ojanen et al., 2013).

Carbon storage of the forest ecosystem is also subject to management practices. When the forest is harvested, most of the carbon stored in wood is rapidly lost to the atmosphere if the harvested wood is used for short-lifetime products such as pulp or energy production (Makrickas et al., 2023). Therefore, a peatland forest, whose soil is a net CO_2 source, has a climate warming impact over the entire forest rotation period, even though it may be a net CO_2 sink at a moment in time.

The most common forest management method implemented in Nordic countries has been Rotational Forestry (RF). In RF, forests are clear-cut when a specific stand volume has been reached and new stands are usually established by planting seedlings on the harvested land (Nieminen et al., 2018). Before planting new seedlings, the harvested land is sometimes fertilized and mounded, and often the mounding material comes from ditch maintenance (Hytönen et al., 2020). Harvest residues (litter, small branches, tree roots and stumps from the previous forest) are often left on the site or removed. Recently, more importance has been given to the investigation and implementation of alternative forestry management methods that would decrease carbon losses from the soil while maintaining profitable timber production. Continuous Cover Forestry (CCF) has been suggested as a management practice that could be applied to reach this goal (Nieminen et al., 2018). In CCF, the forest is never clear-cut as in RF, but rather selectively harvested depending on the forest and soil characteristics, resulting in an unevenly aged forest structure.

In drained peatlands, vegetation growth ~~significantly~~ influences the water table (WT) significantly through evapotranspiration. Increased biomass, particularly from deep-rooted trees, promotes water loss ~~, leading~~ and leads to a decrease in WT (Laiho, 2006). In CCF ~~,~~ the WT remains higher than in the full-grown forest~~(Sarkkola et al., 2010), reducing~~ , because non-harvested mature forest has higher evapotranspiration compared to the forest where a selective harvest has been conducted (Sarkkola et al., 2010). Higher WT in CCF results in reduced peat degradation and ~~minimizing the~~ minimizes carbon loss from the soil. ~~Ditch management costs, which are often necessary after clear-cut, can also be avoided as~~ In CCF, however, the remaining trees ~~in the CCF~~ continue to transpire water ~~, keeping~~ and keep the WT low enough ~~not to hinder tree~~ that WT does not hinder forest growth (Nieminen et al., 2018). ~~An increase in WT could lead to higher anaerobic conditions in the soil layer that promote methanogenesis and eventually even turn drained peatlands into a net CH_4 source (Lohila et al., 2011). Temporal and spatial variations of CH_4 can be attributed to the dynamics of soil temperature, WT and vegetation communities (Minkkinen and Laine, 2006).~~ While in RF, after clearcut, WT rises significantly because of lack of transpiring vegetation (Leppä et al., 2020) and often requires ditch management to lower the WT before planting new seedlings.

The Lettosuo site, a drained nutrient rich peatland forest in Southern Finland, had both selective harvest and clearcut management applied to the site to convert one part of the site into a CCF stand and another part into a RF stand (Leppä et al., 2020) . Measurements of the net ecosystem carbon exchange in Lettosuo showed ~~that mature forest on drained peatland, which was~~ the mature forest to be a small sink of CO_2 before harvest ~~, can become~~ (Korkiakoski et al., 2023). After harvest, RF stand was a bigger CO_2 source ~~after harvest if the site is under RF management compared to CCF (Korkiakoski et al., 2023). Same~~ compared to the CCF stand (Korkiakoski et al., 2023). The same site was a sink for CH_4 ~~due to low WT~~ before harvest (Korkiakoski et al., 2017)~~and~~ , and after selection harvest (Korkiakoski et al., 2020) due to low WT. However, RF stand was a source of CH_4 after ~~harvest (~~clear-cutting ~~, (Korkiakoski et al., 2019))~~due to raised WT (Korkiakoski et al., 2019). An increase in WT could lead to higher anaerobic conditions in the soil layer that promotes methanogenesis and eventually even turn drained peatlands into a net CH_4 source (Lohila et al., 2011). Further, temporal and spatial variations of CH_4 can be attributed to the dynamics of soil temperature, WT, and vegetation communities (Minkkinen and Laine, 2006).

Apart from being a major habitat, peatland systems have challenged terrestrial ecosystem models (Mozafari et al., 2023; Silva et al., 2024), for example because of their dynamic water table regulating carbon processes (e.g., Mezbahuddin et al., 2017), or specific ground vegetation (e.g., Shi et al., 2021). Only in recent years, specific processes for peatlands have been given more consideration (e.g., Liu et al., 2022; Li et al., 2024). The process-based ecosystem model LandscapeDNDC has been used to simulate carbon and water balances in various forest systems, including monoculture (Werner et al., 2012; Dirnböck et al., 2016), structured forests with ground vegetation (Dirnböck et al., 2020; Cade et al., 2021) and managed forests (Grote et al., 2011). The simulations mentioned above considered sites with mineral soils, whereas applications on peat soils are still lacking.

The primary objective of this study is to evaluate the performance of LandscapeDNDC model in forested drained peatlands. To address this objective, we refined and employed a process-based model, applied here for the first time to a nutrient-rich drained peatland in Finland. Refinements to the dynamic WT and high carbon content are investigated using carbon and water flux measurements. We perform a sensitivity analysis to determine the most sensitive parameters for decomposition in carbon rich soil. We assess how variations in tree species composition and management methods influence gas exchange and water balance. The model improvements should allow for a realistic representation of the forest CO_2 and CH_4 budgets, soil hydrology, and soil carbon balances within the drained peatland forest systems. Ultimately, the study aims not only to test the model's applicability and accuracy for Lettosuo study site but also to provide a foundation for assessing future peatland management scenarios. This approach supports the broader goal of identifying climate-smart forest management strategies that contribute to carbon neutrality on drained peat soils.

2 Material and methods

2.1 Model description

The simulation framework LandscapeDNDC (LDNDC) has been developed to allow a flexible problem-specific model composition for the simulation of the water, carbon and nitrogen cycles in cropland, grassland and forest ecosystems (Haas et al., 2013). In this study, the microclimate within the forests is simulated using the sub-model CanopyECM according to Grote et al. (2009). Vegetation related processes are modeled with the Physiological SImulation Model (PSIM) sub-model (Grote et al., 2006, 2011). Soil biogeochemical processes were represented with the MeTr$_{\cancel{x}}^{x}$ sub-model (Kraus et al., 2015), while soil hydrological conditions are represented with the Ecosystem Hydrology (EcHy) sub-model (Dirnböck et al., 2020).

PSIM enables the representation of a multiple species stand, where individual tree species can have their own characteristics and dimensions, while also having interactions with each other (Cade et al., 2021). Including multiple species in the simulation allows to consider the contributions of dominant trees, understorey and ground vegetation to carbon and water fluxes. In particular, the importance of understory in boreal forests has been highlighted before and is thus necessary to be included in the model (Korkiakoski et al., 2023; Leppä et al., 2020).

The soil sub-model MeTr$_{\cancel{x}}^{x}$ accounts for carbon and nitrogen pools and fluxes and their responses to land use and forest management. Most relevant processes considered by MeTr$_{\cancel{x}}^{x}$ for this study are humification, mineralization, nitrification and denitrification as well as CH_4 production and consumption (Kraus et al., 2015). In MeTr$_{\cancel{x}}^{x}$, various litter (Solutes, Cellulose and Lignin) and humus (Labile, Recalcitrant young and old) pools are differentiated according to their chemical structure (Kraus et al., 2015) and carbon to nitrogen ratio, respectively. These are decomposed by microbial pools in the nitrification and denitrification processes. Besides pool size and organic matter properties, processes depend on the availability of oxygen, pH, clay content, and soil temperature and moisture. MeTr$_{\cancel{x}}^{x}$ also covers methane (CH_4) production as a final step at the end of decomposition under anaerobic conditions as well as CH_4 ~~deposition~~transport from air to soil and CH_4 oxidation. Oxygen content is dynamically calculated for each soil layer~~and as well as CH_4 oxidation~~. Detailed descriptions of these processes can be found in Kraus et al. (2015), Molina-Herrera et al. (2015), and Haas et al. (2022).

Soil water dynamics are calculated by the EcHy module, which predicts a dynamic groundwater table (z_{gw}) depending on the simulated water balance. In its conceptual design, EcHy is a one-dimensional (1-D) vertical soil column model. When applying its original version in this study, the simulation domain became waterlogged because precipitation exceeded evapotranspiration and percolation through the lower soil boundary. In reality, however, the site is drained by ditches that induce a lateral water flow component and counteract complete soil saturation. To account for this, a reference water table (Z_{gw}) was introduced, which represents the depth below which no significant lateral flow occurs (e.g., the ditch depth), and the soil is assumed to be fully saturated. In addition, a parameter representing lateral groundwater flow velocity and ditch distance Ψ was implemented. This parameter determines the rate of lateral water loss whenever the simulated dynamic water table depth z_{gw} is above Z_{gw}.

Together, these modifications introduce a lateral (2-D) flow component into an otherwise 1-D framework, enabling EcHy to better reflect local site conditions. Lateral groundwater movement q is given by,

$$q = max(0.0, |Z_{gw} - z_{gw}|) \times \Psi \times K_s \tag{1}$$

z_{gw}: depth of groundwater in m, Z_{gw}: depth of reference groundwater in m, Ψ: Model parameter representing lateral groundwater gradient m^{-1}, K_s ~~is~~ : the saturated hydraulic conductivity of the last soil layer ~~. Negative Z_{gw}, z_{gw} means groundwater table is below soil surface.~~ m min^{-1}.

~~Additionally, the size of the recalcitrant oldhumus pool ($H_{recalcitrant,old}$) was scaled as a function of the soil carbon to nitrogen ratio (~~In the model, soil organic matter is represented by three conceptual pools (labile, recalcitrant young, recalcitrant old) differing in turnover time and C:N ~~). The scaling factor was defined as,~~

$$s(C:N) = 0.8 - \frac{8}{C:N}$$

~~The scaling factor varies between 0 and 0.8. $H_{recalcitrant,old}$ is calculated as,~~

$$H_{\mathrm{recalcitrant,old}}(C:N) = \big(0.9 - s(C:N)\big) \times C:N$$

~~At low~~ ratio. The C:N ratio of the young recalcitrant pool is 1.5 times the bulk soil C:N ~~ratios (nitrogen-rich soils), s(~~ratio, which is the model's default parametrization for agricultural (mineral) soils. Peat soils in this study are characterized by systematically higher bulk C:N ~~) would be negative but the lower limit of scaling factor sets it to zero, resulting $H_{recalcitrant,old}$ would be approximately 0.9 *~~ ratios than mineral soils. For peat, we interpreted the young recalcitrant pool as the main peat pool and therefore aimed to reduce the initial relative share of the old recalcitrant pool compared to mineral soils. To achieve this while conserving bulk soil C and N, we assigned a lower C:N ~~. At high~~ ratio to the old recalcitrant pool than to bulk soil, which reduces the amount of C that is allocated to old recalcitrant pool. The C:N ~~ratios (nitrogen-poor soils) , s(~~ratio of the old recalcitrant pool (CN_{rec}) is scaled as a function of the bulk soil C:N ~~) approaches 0.8 and is capped at this maximum, resulting in $H_{recalcitrant,old}$ to be approximately 0.1 * C: N.~~ ratio (CN_{bulk}):

$$CN_{rec} = \big(0.9 - max(0, 0.8 - 8 \times CN_{bulk})\big) \times CN_{bulk} \tag{2}$$

When CN_{bulk} very large:

$$CN_{rec} = 0.1 \times CN_{bulk} \tag{3}$$

When CN_{bulk} <= 10:

$$CN_{rec} = 0.9 \times CN_{bulk} \tag{4}$$

This formulation therefore reduces the size of the old recalcitrant humus pool with increasing soil C:N ratio. Changes to the model code can be found Shahriyer et al. (2025c).

2.2 Site description

Lettosuo site, located in southern Finland (60°38′31″N, 23°57′35″E), covers a total area of 65 ha (Fig. A1). The site, extensively drained in 1969 using ditches that were 45 m apart, is classified as a nutrient-rich Vaccinium myrtillus type II forest (MtkgII, Laine (1989)). Lettosuo was originally a sparsely treed, mesotrophic pine-birch sedge fen rich in herbs (Korkiakoski et al., 2023). Fertilizers were used after drainage to help with the growth of existing pine (*Pinus Sylvestris*) trees. In the 1970s and later, some thinning was done to ensure better growth of pine, but those thinning information are unavailable. Over time Lettosuo became a mixed forest site, where pine and birch (*Betula Pendula*) formed the overstory and spruce (*Picea Abies*) formed the understory canopy. The forest floor consisted of various herbs, shrubs and graminoids (Korkiakoski et al., 2023).

The site was divided into three sections according to the applied management methods: a control stand where no management action had taken place; a Continuous Cover Forestry (CCF) stand where all the pine trees (75 % of the original total biomass) were harvested in March 2016 (Korkiakoski et al., 2020); and a Rotational Forestry (RF) stand where all the trees were removed by clear-cutting, also in March 2016 (Korkiakoski et al., 2019).

In RF, the application of heavy harvesting machinery destroyed the ground vegetation, while in CCF, ground vegetation was only affected on logging trails. In RF, the harvest residues were left at the felling area, while in CCF, the harvest residues were placed on the logging trails. At RF, ditches were maintained after clear-cut and peat extracted from ~~nearby ditches during ditch maintenance were~~ the ditches was used to form mounds of peat soil ~~and~~ where new spruce seedlings were planted ~~on top of the mounds~~ in 2017. Most of the spruce seedlings died ~~off~~ during the drought in 2018 (Korkiakoski et al., 2023). Later ~~as a result the stand became birch-dominated from the~~ naturally occurring birch seedlings became the dominant species at RF stand.

2.3 Site observations and auxiliary data

2.3.1 Model driving data

Finnish Meteorological Institute's long-term (1963-2021) observation-based meteorological data were used to drive the model (Aalto et al., 2016). Meteorological data consisted of temperature, precipitation, global radiation, wind speed and relative humidity. Nitrogen deposition, in the form of ammonium and nitrate wet deposition, was selected to match values (6 kg ha^{-1} y^{-1}) for the northern latitudes (Harmens et al., 2011). Background methane concentrations were set at a constant value of 1.74 ppb. ~~RCP4.5 midyear CO_2 concentration was used for CO_2 concentration, which were gapfilled and bias-corrected towards observed~~ The CO_2 concentration used to drive the model was based on observations up to 2005 and follows RCP4.5 since then (i.e. historical + scenarios) and deviates from the observed value by 1.3 ppm by 2021 (Meinshausen et al., 2011).

2.3.2 Model evaluation data

One-sided Leaf Area Index (LAI) was estimated from Sentinel-2 satellite data for all stands and mostly consisted the post harvest years (Nevalainen, 2022; Korkiakoski et al., 2023). Additionally, the modeled pre-harvest LAI was compared against site estimated LAI reported by Leppä et al. (2020).

Data from the control stand included CH_4 fluxes, which were measured with six automatic chambers from June 2015 to January 2019. WT measurements at control stand covered the years 2016-2021 (Korkiakoski et al., 2020). The soil moisture content measurements at depths of 10 cm and 20 cm covered the duration from July 2015 to January 2019.

Eddy-covariance (EC) measurements of CO_2 exchange between the ecosystem and the atmosphere, i.e. net ecosystem exchange (NEE), were conducted on top of a telescopic mast (height 25.5 m until June 2019 and later at 27.2 m) at ~~continuous cover~~ CCF stand. NEE before selective harvest will be referred to as pre-harvest and after selective harvest will be referred to as $CCF_{postharvest}$. The pre-harvest data covered the time period from January 2010 to March 2016 and $CCF_{postharvest}$ from April 2016 to December 2021. Gross primary production (GPP) and total ecosystem respiration (TER) were estimated from the NEE data (Korkiakoski et al., 2023) and used in this study to evaluate the LDNDC model performance. CH_4 measurements from the CCF stand were conducted with six automatic chambers from May 2015 to May 2018 (Korkiakoski et al., 2020), i. e. one year before the harvest and three years after the harvest. These were used to validate the CH_4 fluxes from CCF simulation. CCF also had continuous WT measurement from January 2010 to December 2021 (Korkiakoski et al., 2023).

A separate EC tower (height 3.2 m) in the rotational forestry stand was set up after the clear-cut harvest in March 2016 (Korkiakoski et al., 2019). NEE measurements from the RF after clear-cut, will be referred to as the $RF_{postharvest}$. NEE, GPP, TER and WT data from April 2016 to December 2021 were used in this study. CH_4 fluxes were measured with the manual chambers and covered the period of May 2016 to September 2017 (Korkiakoski et al., 2019).

2.4 Simulation setup

In the simulations, the vertical soil profile was divided into several layers of increasing thickness with increasing layer depth (Table 1). The carbon and nitrogen content, bulk density and pH of the soil layers were taken from the measured Lettosuo data previously reported by Leppä et al. (2020) and Korkiakoski et al. (2017). These soil variables and their prescribed initial levels are given in Table 1.

The simulations started from a pristine peatland condition in 1969. Fluctuations in litter and humus pools after initialization were stabilized during the first three simulation years. During this period, the Z_{gw} was set to 0.01 m depth to stabilize the soil carbon pools for pristine peatland condition. In the case of pristine peatland simulation, to study the soil carbon changes, the Z_{gw} was kept at 0.01 m until 2021. Otherwise, for forest stand simulations, Z_{gw} was set to 0.62 m after initial three years to represent drained peatland conditions. The model then simulated WT dynamically with the modification described in Section 2.1.

The initialization of tree species and forest floor vegetation is presented in Table 2. The simulation began in 1969 with pine trees and the forest floor vegetation. Birch and spruce were added in 1971 and 1972, respectively. Management events

Table 1. Soil layer profile from the measured Lettosuo data previously reported by Leppä et al. (2020) and Korkiakoski et al. (2017) for the simulation, where soil depth in cm, Carbon (C) content, Nitrogen (N) content, Bulk density (BD), Carbon to Nitrogen ratio (CN), pH, Van Genuchten parameter n and (α), and minimum water filled pore space ($WFPS_{min}$), are given as,

Soil depth (cm)	C (%)	N (%)	BD (kg dm^{-3})	C:N	pH	n	α (m^{-1})	$WFPS_{min}$ (%)
0-10	55	2.22	0.14	24.77	3.0	3.0	8.0	0.25
10-30	55	2.22	0.14	24.77	3.0	3.0	8.0	0.70
30-60	55	2.22	0.14	24.77	3.0	3.0	8.0	0.90
60-90	55	2.22	0.15	24.77	3.5	3.0	8.0	0.90
90-190	58	2.42	0.20	23.96	4.5	3.0	8.0	0.98

Table 2. Individual species were introduced to the simulation starting from 1969. No species were removed for non-managed control and continuation of certain species until the end is indicated by –. Pine was removed for Continuous Cover Forestry (CCF) during selective harvest and all species were removed in the Rotational Forestry (RF) during clear-cut (RF_{CC}). Individual species were reintroduced for a new forest in RF ($RF_{Newforest}$) with number of seedlings $RF_{Newforest,n}$ reported in Korkiakoski et al. (2019).

Species	Initiation	Initial$_{n\ ha^{-1}}$	Control	CCF	RF_{CC}	$RF_{Newforest}$	$RF_{Newforest,\ n\ ha^{-1}}$
Pine	01/01/1969	535	–	01/03/2016	01/03/2016	01/04/2017	1520
Spruce	01/01/1972	1400	–	–	01/03/2016	01/04/2017	1120
Birch	01/01/1971	800	–	–	01/03/2016	01/01/2019	17400
Forest floor	01/01/1969		–	–	–	–	–

(selective harvest and clear-cut) took place in 2016. Harvest residues were left in the simulation domain and stemwood biomass was removed after management events. All simulations were run until end of 2021. All the modules were run with a sub-daily time step (30 minutes) and sub-daily and daily simulation outputs were used for various investigations.

The sensitivity of NEE to soil decomposition was tested (described in section 2.6 and Appendix A2) for a range of soil ~~decomposition~~ parameters (Table A1). ~~Several of those sensitive soil parameters related to the decomposition of different humus and litter pools were later adjusted during forest stand simulations (Table A2).~~ Species parameters reported in Grote et al. (2011), a study which simulated a mixed forest stand consisting of pine, spruce and birch trees on mineral soil in southern Finland, were used and adjusted to run the sensitivity test simulations and full forest simulations for this study (Table A2). These parameters included e.g. photosynthesis related VCMAX (Maximum RubP saturated rate of carboxylation at 25°C for sun leaves), KM20 (Maintenance coefficient at reference temperature), SLAMAX (Specific leaf area in the shade) and SLAMIN (Specific leaf area in the full light). Several sensitive soil parameters related to the decomposition of different humus and litter pools were later adjusted during full forest simulations (Table A3).

2.5 Model data analysis and evaluation

The correlation coefficient (r) and Nash-Sutcliffe efficiency (NSE) were calculated from the daily aggregate of the available measurements and corresponding modeled data. NSE values can vary from $-\infty$ to 1. Model output that produces an NSE value of 1 is described as the perfect simulation~~. Preferably NSE values greater than 0.5 are desirable, indicating good model performance~~, thus NSE values closer to 1 are desirable.

NSE is defined as,

$$NSE = 1 - \frac{\sum_{i=1}^{n} \left(Q_{o_i} - Q_{m_i}\right)^2}{\sum_{i=1}^{n} \left(Q_{o_i} - \overline{Q_o}\right)^2} \tag{5}$$

Where, Q_o represents the observed data at time i, Q_m represents the modeled data at time i, $\overline{Q_o}$ is the mean of the observed data. n is the total number of observations.

We further used Root Mean Square Error (RMSE) to quantify the differences ~~in NEE and WT~~ between the model and the observations for NEE and WT. In this analysis, seasons are defined as December–January (winter), March–May (spring), June–August (summer) and September–November (autumn).

Since a single simulation setup was used for all three forest stand simulations before the harvesting events, both measured and simulated data will be referred to as pre-harvest data (2010–2015). Korkiakoski et al. (2023) calculated the Annual CO_2 balances (NEE, GPP and TER) for 2016 from April 2016 to March 2017 and the modeled estimates for 2016 ~~was~~ were also calculated similarly in the CCF$_{postharvest}$ and RF$_{postharvest}$. To show the sensitivity of the simulated CH_4 flux with WT after clear-cut harvest, the groundwater lateral gradient parameter was changed (28.7 m^{-1} to 38.7 ~~, Table A2~~m^{-1}, Table A3) in the simulation to reproduce the lowest and highest observed WT at RF (section 3.3).

The effect of drainage on the simulated soil carbon (SC) storage was compared to the SC loss reported by (Simola et al., 2012). The influence of harvesting, under different management methods, on SC dynamics was assessed by quantifying changes in SC following harvest. This included investigating the partition of different litter (solutes, cellulose and lignin) and humus (labile, recalcitrant young and old) pools. The evolution of the total carbon (soil carbon + carbon in vegetation) over the whole simulation period was also studied (section 3.5). A pristine peatland simulation, without any drainage or harvesting, served as a reference. Data and ~~python~~ Python codes used in this study can be found from ~~Shahriyer et al. (2025a)~~ Shahriyer et al. (2025a, 2026a, b).

2.6 Sensitivity test

Sensitivity tests for soil ~~parameter~~ parameters were carried out separately with mature forest stands in 1-year simulation runs. ~~Soil parameters and their range selected for the sensitivity tests are given in Table A1. The fixed species parameters used in the sensitivity tests are given in Table A2.~~ For sensitivity testing, the Python library SPOTPY and its FAST algorithm was used (Houska et al., 2015, 2017). Soil parameters~~were separated~~ ~~,~~ , divided into three sets ~~,~~ and each consisting of nine parameters~~(~~, and their range selected for the sensitivity tests are given in Table A1~~)~~. The sets consisted of decomposition constants for different soil pools, factors related to dependency on conditions for decomposition and factors related to the humification of different soil pools. ~~With this setup, the simulation was run~~ The three sets of nine parameters were not varying simultaneously; instead, only values of one set of nine parameter were varied at a time. During these sensitivity tests fixed values of species parameters were used and they are given in Table A2. First, the nine soil decomposition-related parameters in set 1 were run for 8649 ~~times (Houska et al., 2017) for each set of parameters, and the soil parameter values~~ times (Houska et al., 2017). The values of these parameters were randomly selected by the FAST algorithm. ~~FAST algorithm indicates~~ For first set run, set 2 and 3 parameters had default values (Table A1). At the end of the run FAST algorithm indicated the sensitive parameters ~~in the parameter sets~~within the first parameter set.

~~First, sensitivity among the parameters related to the decomposition was tested. Further,~~ After first set of runs, in order to proceed from one set of parameters to the next, we compared the simulation output of NEE from the sensitivity test runs with measured NEE values. ~~Within~~ The parameter values that produced the best NSE in a single run, within the range of minimum and maximum parameter values, ~~the parameter value that produced the best NSE was selected and~~ were selected (Table A1). These were subsequently used as fixed parameter values for first set of soil parameters when the ~~next~~ sensitivity test for the second set of nine soil parameters was ~~run. A similar procedure was followed for the third parameter set. The~~ conducted. During the second set of runs parameters in set 3 had default values. Again, the parameters values that produced the best NSE (related to NEE), in a single run, were selected from the second set. Now these eighteen parameters had values fixed when the third sensitivity test for set 3 was conducted (Table A1). Again parameter values for best NSE in a single run for third set are given in Table A1. We consider the number of simulations per set of parameters to be adequate and the results of these tests are given in the Appendix (~~Fig. A2-4~~Table A1, Fig. A2 - A4 and Fig. S1 - S3).

The parameter related to the decomposition of recalcitrant young humus was the most sensitive in the first set of sensitivity tests (Fig A2). Other sensitive parameters in this set were related to the decomposition of labile humus, recalcitrant old humus, raw litter and the dependence of decomposition on litter lignin concentration. In the second set of parameters, parameters related to temperature, pH and decomposition reduction due to anaerobicity were found to be sensitive (Fig. A3). The parameters related to C:N ratio of the old humus pool to the total soil C:N ratio, the humification of the recalcitrant young humus, dissolved organic carbon, active organic material and solutes were the most sensitive parameters in the third set (Fig. A4).

~~According to the results of the parameter sensitivity tests, parametersrelated to the temperature dependency of decomposition, decomposition of raw litter and wood, decomposition constants for three humus pools. Their values~~ The sensitivity analysis was conducted purely to observe the sensitivity of the parameters, and no optimized parameter values were used in full forest simulations as such. Full simulations from seedlings to maturity were done separately with only a few select soil parameters, and the parameter values were chosen as such that maintain the observed species composition (Table A3). Species parameters used in full forest simulation are given in Table A2. Careful consideration was given to full forest simulations, as slightly different parameter values could produce a different composition of forest compared to what had been observed at the site. Our goal requires that the simulation produce the observed forest structure. Several variables, NEE, soil moisture, water table, LAI and forest structure, CH_4, were compared to the measurements in the full forest runs as opposite to the sensitivity runs where

Table 3. Comparison between simulated vegetation structure with observations before management at stand age of 45 years (08/2014). Simulated outputs are shown in bold. Tree numbers (n ha^{-1}), tree heights and stand volumes collected (Korkiakoski et al. (2023)) from Lettosuo site are given in parenthesis. SD is the standard deviation. Simulated individual tree species diameters are given in bold. LAI estimates for individual species reported by Leppä et al. (2020) are given in parenthesis.

Vegetation	Trees (n ha^{-1} $\pm$ SD)	Height (m)	Volume (m^3 $\pm$ SD)	Diameter (cm)	LAI (m^2 m^{-2})
Pine	**488** (494 $\pm$ 11)	**17.1** (20)	**203** (184 $\pm$ 13)	**25.2**	**1.80** (1.92)
Birch	**733** (765 $\pm$ 32)	**13.2** (13)	**38** (52 $\pm$ 1)	**9.8**	**1.19** (1.12)
Spruce	**1285** (1252 $\pm$ 80)	**8** (7–10)	**30** (32 $\pm$ 11)	**7.8**	**1.69** (1.62)
Forest floor	–	–	–	–	**0.94** (1)

only NSE related to NEE was checked. Setting up the optimization of the full forest runs with all the investigated variables might be possible, but the full runs were computationally time consuming.

3 Results

3.1 Development of forest structure before and after management

In the forestry stand simulations, the simulated forest stand at age 45 showed the number of trees of individual species was within the range of observations (Table 3). The height of the individual species was also close to the observed values. The modeled pine and spruce volumes were close to the range of observed volumes, while birch had 27% less volume. Modeled LAI of different species matched well with reported LAI before harvest in 2014 (Fig. 1a). The modeled LAI of 0.94 m^2 m^{-2} for forest floor vegetation in August 2014 was similar to the LAI of 1 m^2 m^{-2} reported by Leppä et al. (2020). The same literature reported LAI for above ground canopy (pine + spruce + birch) to be 4.66 m^2 m^{-2} and the corresponding modeled LAI was 4.68 m^2 m^{-2} (August 2014; Table 3).

Modeled pine and spruce LAI were diminishing from 2016 to 2021 for control simulation (Fig. 1b), which was not seen in the prior six years (Fig ~~S1~~S4). The sum of pine and birch modeled LAI was closest to the satellite-based LAI (Fig. 1b), and this could be realistic since pine and a small percentage of birch were forming the upper-story canopy in the control stand. The decrease in LAI, similar to control, was not seen in the CCF simulation. Infect spruce LAI was increasing up to 2021 because of the removal of the pine during harvest and ~~infect spruce LAI was increasing up to 2021~~ ideal growing conditions for spruce (Fig. 1c). Spruce LAI during summer months was closer to satellite-based LAI, while the sum of spruce and birch modeled LAI was always larger than the satellite-based LAI (Fig. 1c). The modeled LAI for birch and forest floor remained consistent from 2016 to 2021 for both control and CCF. After clear-cutting in RF, the modeled LAI was almost double the satellite-based LAI in 2016, whereas the discrepancy between the two decreased progressively after 2018 (Fig. 1d). Simulated birch and forest floor LAI were closest to satellite-based LAI in 2019 to 2021 (Fig. 1d).

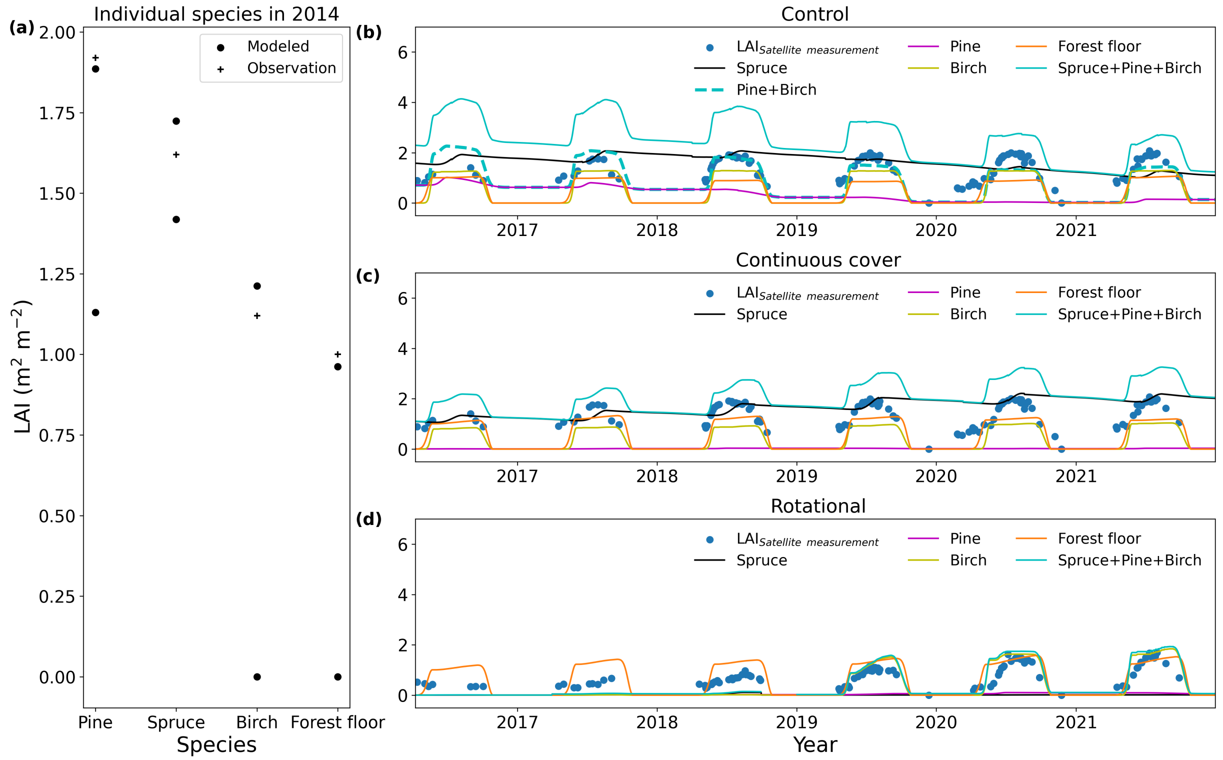

Figure 1. (a) Comparison of individual species one-sided Leaf Area Index (LAI) estimates from field observations (plus) (Leppä et al., 2020) with minimum and maximum modeled LAI (circles) in 2014 for a 45-years-old forest. **(b)**, **(c)** and **(d)** show LAI development in different management scenarios and one-sided LAI comparisons between the model (solid and dashed lines) and satellite-estimated LAI (blue dots). The Pine+Birch LAI only for the control **(b)** are shown with dashed lines.

3.2 Dynamics of soil moisture, water table

Soil moisture dynamics were simulated well for 2015–2017 (May - September), but there were some differences between the model and measurements in 2018 (Fig. 2). The model captured the dynamics of 10 cm soil moisture for 2016 and 2017 best. However, in 2015, the ~~model~~ modeled 10 cm soil moisture was slightly lower compared to the measurements and in 2018, the modeled 10 cm soil moisture was higher compared to the measurements. For 20 cm depth, the model produced the best results for 2015–2017 but from July 2018 onward, model overestimated the soil moisture.

The modeled WT in the pre-harvest years (2010-2015) were similar to the observations conducted at the CCF stand (Fig. 3a). The simulation showed large deviations from the measured mean in especially during summer and autumn in 2016 and 2017 (See also Fig. ~~S2~~S5). From 2018 onward the modeled WT in CCF stand was again similar to the observed WT. The model also predicted the control stand WT within the observed range and reflected the observed dynamics (Fig. 3b). The largest differences in the control stand occurred in the autumn in 2018 and 2019 (See also Fig. ~~S3~~S6). WT comparison between the model and observations at the RF stand also showed that the simulated WT following the observed dynamics (Fig. 3b) had

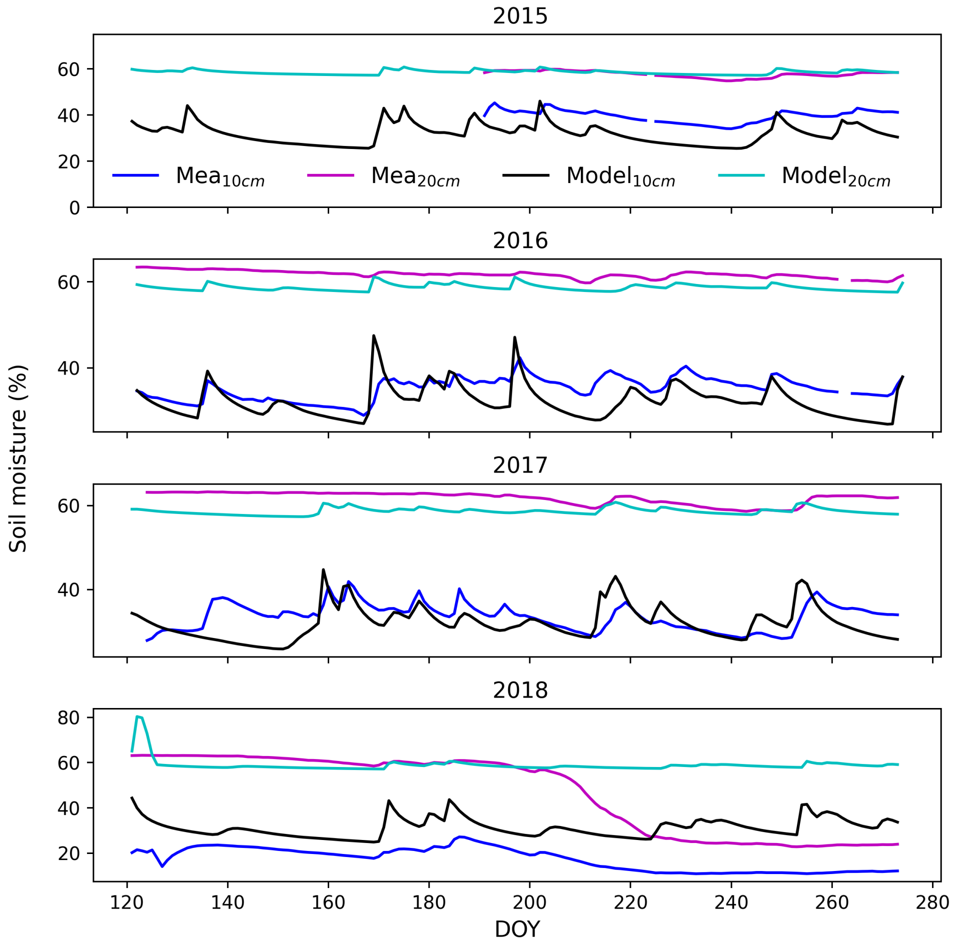

Figure 2. Simulated and measured soil moisture (volumetric moisture content) for the control stand from the beginning of May to the end of September shown in day of year (DOY). Blue and magenta lines show measured soil moisture at 10 and 20 cm depths, respectively. Black and cyan lines show the simulated soil moisture at 10 and 20 cm depths, respectively.

much lower differences between model and measured WT (Fig. ~~S4). Modeled~~ S7). Similar to observation modeled WT rises after clear-cut at RF stand due to the removed transpiring biomass, while rise in WT from selective harvest at CCF stand was not significant (Fig. ~~S5).~~ 4). The initial (2016 and 2017) discrepancy in CCF WT after harvest disappears in the later years.

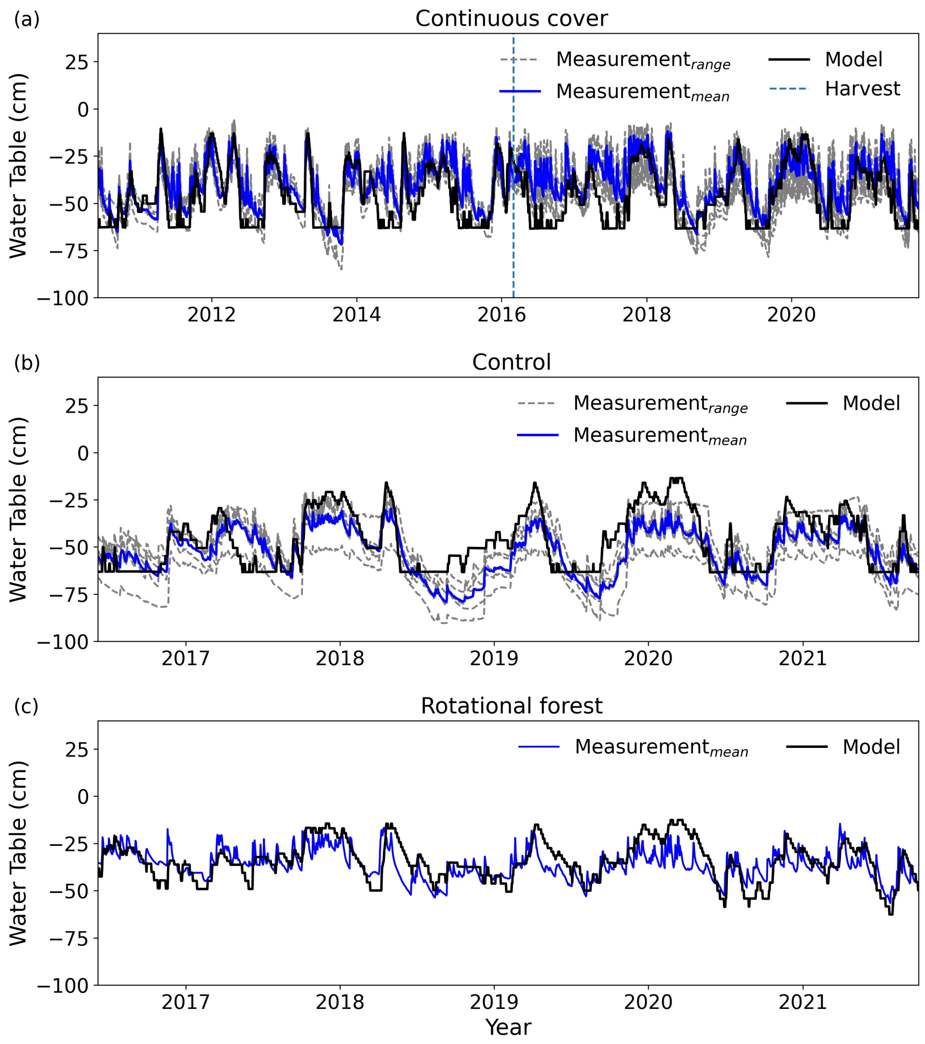

Figure 3. Water table (WT) dynamics in the **(a)** continuous cover forestry stand (CCF, includes pre-harvest and post-harvest WT), **(b)** control stand and **(c)** rotational forestry (RF) stand. Blue and black lines represent the mean measured and simulated WT depth, respectively. Gray dashed lines show the range of measured WT from different WT loggers at the CCF and control stand. The blue vertical dashed line shows when the selective harvest took place at the CCF stand. Negative values represent WT below the soil surface.

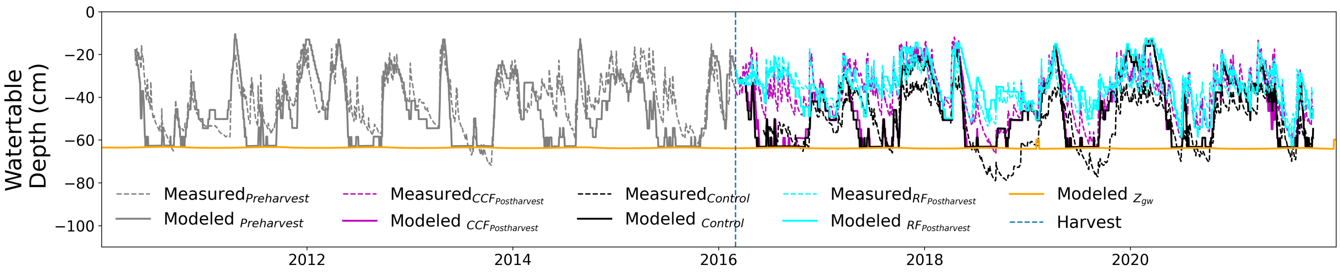

Figure 4. Modeled (solid) and measured (dashed) water table at pre-harvest (gray), Control (black), $CCF_{postharvest}$ (magenta), $RF_{postharvest}$ (cyan) conditions. Additionally the reference water table (Z_{gw}) shown in orange and vertical dashed line shows the time of harvest.

3.3 Methane flux comparison and sensitivity with water table

Manual chamber measurements showed RF stand to be a source of CH_4 in summer months after clear-cut harvest. ~~As the~~ The simulations originally showed CH_4 sink for the same period~~,~~. As temporal and spatial variations of CH_4 can be attributed to the dynamics of WT, soil temperature and vegetation communities (Minkkinen and Laine, 2006) and in dry conditions to the wind speed (Korkiakoski et al., 2017) and soil temperature (Sundqvist et al., 2014), only the role of WT on the CH_4 flux difference was further investigated. Indeed, the CH_4 flux in the model was found to be sensitive to the WT variations after clear-cut. ~~The~~ To simulate two different WT, the groundwater lateral gradient parameter ~~was modified to simulate WT similar to the lowest and highest observed WT at the RF stand in two RF simulations (Fig. 4) . In these simulations, simulated WT were similar before the clear-cut but changed after the~~ (Ψ) was modified while keeping the reference WT (Z_{gw}) same. Modification to Ψ did not change the simulated WT before clear-cut, but simulated WT did indeed changed after clear cut. No additional changes were needed for the model setup to produce the shift in WT.

The two simulated WT were also similar to the lowest and highest observed WT at the RF stand (Fig. 5). Simulation with the original value ~~of groundwater lateral gradient parameter, that~~ (Ψ = 28.7 m^{-1}, Table A3), produced the lowest WT, led to a higher sink of CH_4. While the modified parameter value (Ψ = 38.7 m^{-1}) produced a higher WT and resulted in smaller sink of CH_4. In high WT simulation, the site was even a source of CH_4 on some occasions. ~~Both~~ Modeled CH_4 fluxes in both RF simulations showed very little changes ~~in modeled CH_4 fluxes~~ before harvest and ~~the model simulated~~ represented a lower CH_4 sink compared to the measurements (Fig. ~~4~~5).

~~Modeled~~ For both control and CCF stand modeled CH_4 flux was within the variation of the automatic chamber measurements ~~for both control and CCF stand~~ (Fig. ~~5~~6). The measurements showed mostly uptake of CH_4 from the atmosphere over the 3.5 years of measurements at both stands. When looking at the seasonal dynamics, compared to the measurements, the model was in the upper end of CH_4 uptake during spring and summer, while the model underestimated the uptake during autumn and early winter. Korkiakoski et al. (2017) showed that CH_4 flux aligned with soil temperature at the beginning of summer and with WT from the mid-July onward at this site. However, the underestimation of uptake was not clearly evident in 2016 for either stand.

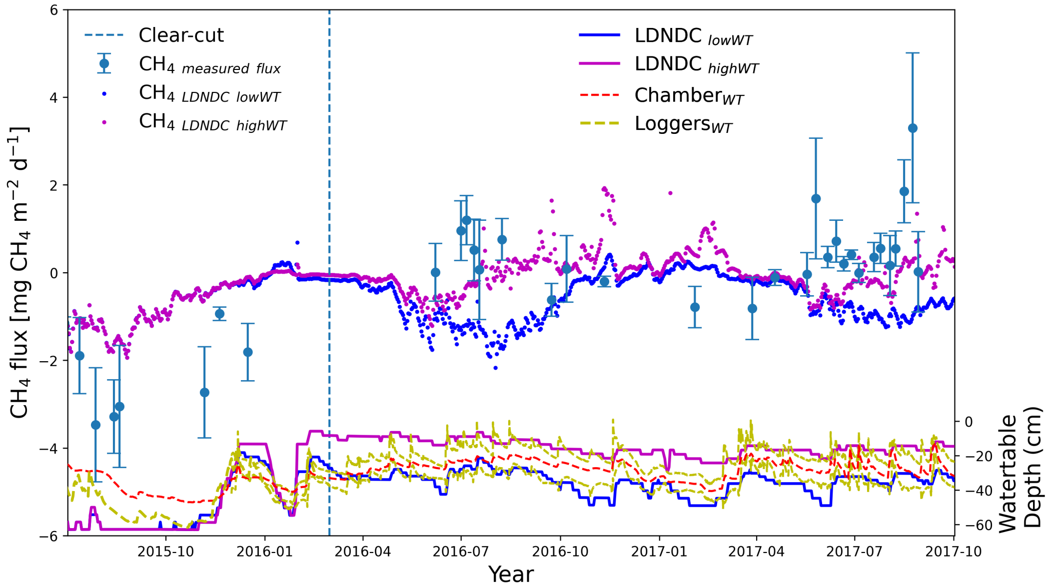

Figure 5. Manual chamber CH_4 flux measurement is represented by light blue dots and associated standard deviation shown with the bars. The highest and lowest Water Table (WT) observed from automatic WT loggers at the rotational forestry (RF) stand are shown in yellow dashed line. WT measured along manual chamber is given in red. Low and high-WT, simulated by modifying groundwater lateral gradient parameter (Ψ), shown at the bottom by darker blue and magenta, respectively. Corresponding modeled CH_4 fluxes are shown at the top with darker blue and magenta dots, respectively. Vertical dashed blue line shows the timing of the clear-cut harvest at RF.

3.4 Ecosystem CO_2 exchange before and after management

The model captured the NEE better in the pre-harvest ~~simulation~~ (r = 0.88, NSE = 0.75, slope = 0.92) than in either $CCF_{Postharvest}$ and $RF_{Postharvest}$ (Fig. ~~6a~~ 7a - c). Performance for modeled GPP was similar for both pre-harvest and $CCF_{postharvest}$, while $RF_{postharvest}$ had a lower NSE (0.75) and higher slope (1.26) to the fitted line (Fig. ~~6d~~ 7d - f). A similar comparison for TER showed that the modeled TER performed well in all three simulations (r = 0.94 - 0.96, NSE = 0.87 - 0.92, Fig. ~~6g~~ 7g - i). ~~The complete daily time series with gapfilled measurements and model results are given in supplementary section 3 (see also Fig. S6-11 and Fig. S12 for a half hourly comparison~~

The modeled NEE (NEE_{mod}) was better after calibrating the WT than the NEE estimated from the simulation with reference WT ($NEE_{Z_{gw}}$) (Fig. S8a). The calibrated NEE_{mod} was similar in magnitude and temporal dynamics as EC based (NEE_{EC}) with some minor discrepancies in pre-harvest condition. Highest RMSE 9.5 $g\,CO_2\,m^{-2}\,d^{-1}$ in the NEE_{mod} was in the summer 2010 (Fig. S9). High spring, summer and autumn RMSE values were also observed in 2014 compared to other years. Model is simulating similar seasonality for GPP and TER compared to EC based estimates (Fig. S8b and c, respectively). Highest discrepancy was observed in summer 2014 for GPP_{mod} (RMSE 17.1 $g\,CO_2\,m^{-2}\,d^{-1}$ Fig. S9). Model captured the TER well other than the high respiration peaks in the summer of 2010 and 2013. The model was also producing slightly higher

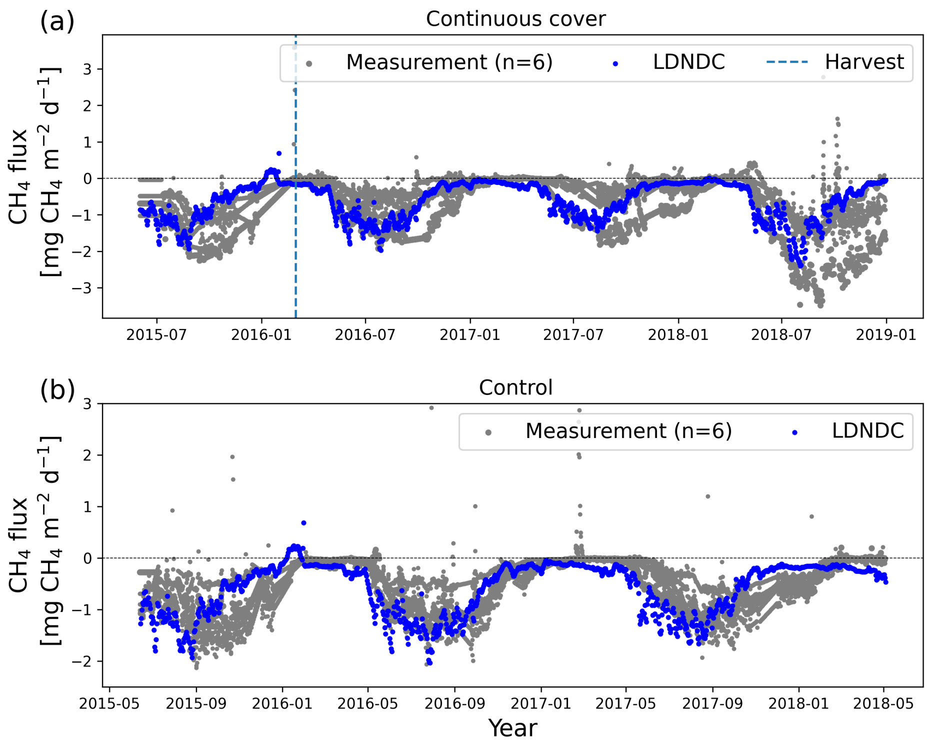

Figure 6. Time series of modeled (blue) CH_4 flux and 6 automatic chamber measurements (gray, n=6) conducted at the **(a)** continuous cover forestry (CCF) and **(b)** control stand. Vertical dashed blue line in **(a)** shows the selective harvest at CCF.

winter respiration compared to what was estimated from observations in the beginning of 2013 (Fig. S8c). Highest RMSE in TER_{mod} was observed in summer of 2010 and 2014 (Fig. S9).

After the selective harvest in 2016, NEE was simulated well for 2017, 2020 and 2021. To an extent, this was also true for late summer and autumn 2018 and 2019, except that the model produced higher uptake (NEE) in spring and early summer for those years (Fig. S10a). 2016 summer and autumn had noticeable deviation in NEE, while GPP was overestimated by the model and TER was underestimated (Fig. S10b and c, respectively). In spring and early summer 2018 and 2019, GPP and TER were overestimated by the model. Summer RMSE for NEE_{mod} varied around $6-8\ g\ CO_2\ m^{-2}\ d^{-1}$ and other seasons it was lower than $6\ g\ CO_2\ m^{-2}\ d^{-1}$ and most of the time it was lower than $4\ g\ CO_2\ m^{-2}\ d^{-1}$ (Fig. S11). Highest RMSE in GPP_{mod} was observed in 2018 summer and in TER_{mod} it was 2019 summer.

NEE_{mod} after clear-cut captured the gradual transition from higher daily net source during the first three years after harvest to lower daily net source or sometimes even sink, during the summer season, in the next three years (Fig. S12a). NEE_{mod} had the best agreement with measurements 2019-2021 and, to an extent, Autumn 2018. NEE from May-August in 2016 and 2017 were underestimated by the model and indicated ecosystem being a smaller source of CO_2 compared to the measurement. The GPP_{mod} was similar to the GPP_{EC} for 2016–2019, while the GPP for late spring and early summer 2020 and 2021 was slightly overestimated by the model (Fig. S12b). TER_{mod} was underestimated compared to the TER_{EC} for the summers of 2016 and 2017 and overestimated for late springs and early summers of 2020 and 2021. 2018 and 2019 TER was represented by the model (Fig. S12c) and highest RMSE in TER_{mod} was in 2021 (Fig. S13).

On the annual scale, ~~the modeled NEE (NEE~~$\cancel{_{Mod}}$~~)~~ NEE_{mod} was similar to the EC-measured NEE~~(NEE~~$\cancel{_{EC}}$ ~~)~~ in both pre-harvest and post-harvest conditions with some exceptions. The largest discrepancy in $NEE_{\cancel{Mod}\,mod}$ was seen in 2014 followed by 2012 during pre-harvest years (Fig. ~~7a~~8a), and first post-harvest year (4/2016 - 3/2017) of both CCF (Fig. ~~7b~~8b) and RF (Fig. ~~7c~~8c). In $CCF_{postharvest}$, $NEE_{\cancel{Mod}\,mod}$ was a net source of CO_2 for the first three years after selective harvest, similar to the NEE_{EC}. $NEE_{\cancel{Mod}\,mod}$ was a sink of CO_2 from the fourth year onward, same as the NEE_{EC}. In the $RF_{postharvest}$, the $NEE_{\cancel{Mod}\,mod}$ indicated the ecosystem was a source of CO_2 ~~. NEE~~$\cancel{_{Mod}}$ and NEE_{mod} is similar to the NEE_{EC} for the six post-harvest years after clear-cut. Both modeled and observed annual ecosystem CO_2 emissions decreased over time after the clear-cut.

In the pre-harvest, ~~modeled GPP(GPP~~$\cancel{_{Mod}}$~~)~~ GPP_{mod} was similar in magnitude to the ~~EC based GPP (~~GPP_{EC} ~~)~~ and the biggest difference was in 2014, when $GPP_{\cancel{Mod}\,mod}$ was 35% higher (Fig. ~~7d~~8d). In the $CCF_{postharvest}$, $GPP_{\cancel{Mod}\,mod}$ had a similar pattern compared to the GPP_{EC} and the largest difference taking place in 2018, when the $GPP_{\cancel{Mod}\,mod}$ was 44% higher than the GPP_{EC} (Fig. ~~7e~~8e). In the $RF_{postharvest}$, the $GPP_{\cancel{Mod}\,mod}$ ranged from 21% lower (2018) to 24% higher (2021) compared to the GPP_{EC} (Fig. ~~7f~~8f). In the pre-harvest condition, ~~modeled TER (TER~~$\cancel{_{Mod}}$~~) and EC-based TER (~~TER_{mod} and TER_{EC} ~~)~~ did not show much difference in the balances (Fig. ~~7g~~8g). In $CCF_{postharvest}$, $TER_{\cancel{Mod}\,mod}$ was higher in 2018 (28%) and 2019 (26%) (Fig. ~~7h~~8h), and in $RF_{postharvest}$, $TER_{\cancel{Mod}\,mod}$ ranged from 16% lower (2017) to 22% higher (2021) compared to the TER_{EC} (Fig. ~~7i~~8i).

3.5 Management effect on soil carbon storage

Simulated SC storage started to decrease after drainage and continued until the management events (Fig. ~~8~~9). In contrast, pristine peatland with no drainage showed a small accumulation of SC assuming a conservative ground vegetation coverage of 40% of the total area. The development of SC after the harvest varied among the managements and depended on the management method. In control, where no trees were removed, SC continued to decrease until the end of the simulation. In CCF, where the forest was partially removed, SC accumulated for a couple of years likely due to the carbon input from harvest residue, after which it started to decrease again, although SC remained higher than in control. In RF, where all trees were removed, the SC increased for few years likely due to the carbon input from harvest residue and then started to decrease, but SC remained higher than in both control and CCF. Annual SC loss for 2010–2015 ~~period~~ was 233 g C m^{-2} y^{-1}. SC loss for 03/2016–2021 ~~period~~ was 221 g C m^{-2} y^{-1} in control, 95 g C m^{-2} y^{-1} in CCF, and SC gain 79 g C m^{-2} y^{-1} in RF.

The difference between total carbon (TC) and SC in pristine was small and owing to a relatively small amount of carbon stored in the vegetation (Fig. ~~8~~9). After the drainage, TC decreased for all forestry simulation scenarios since there was more carbon lost from the soil compared to the carbon accumulated by the vegetation. With continued forest growth, trees accumu-

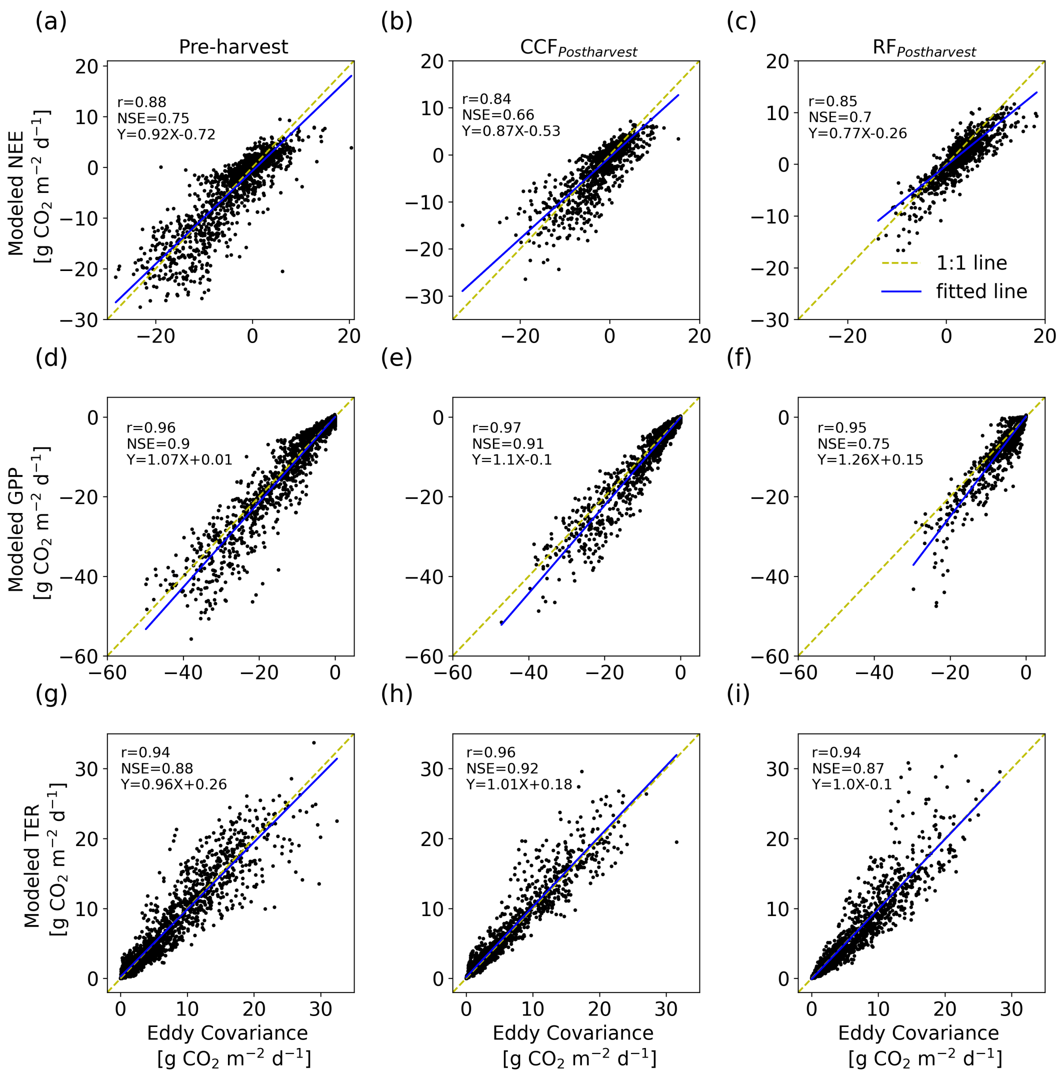

Figure 7. Modeled versus measured NEE (a-c), GPP (d-f) and TER (g-i) for pre-harvest (a, d, g) and post-harvest conditions of the continuous cover forestry (CCF; b, e, h) and rotation forestry (RF; c, f, i) stand. Correlation coefficients (r) and Nash–Sutcliff model efficiency (NSE) given in the figures show agreement among the variables compared. Yellow dashed lines and blue lines are the 1:1 lines and fitted lines, respectively. The equations for fitted lines are given as Y. For this comparison, the instances when measurement data were missing, the corresponding modeled time periods were removed and then daily sums were taken for both. Thus these data represented here does not include the true daily sum and the gapfilled daily time series is shown in Fig. S8, Fig. S10 and Fig. S12.

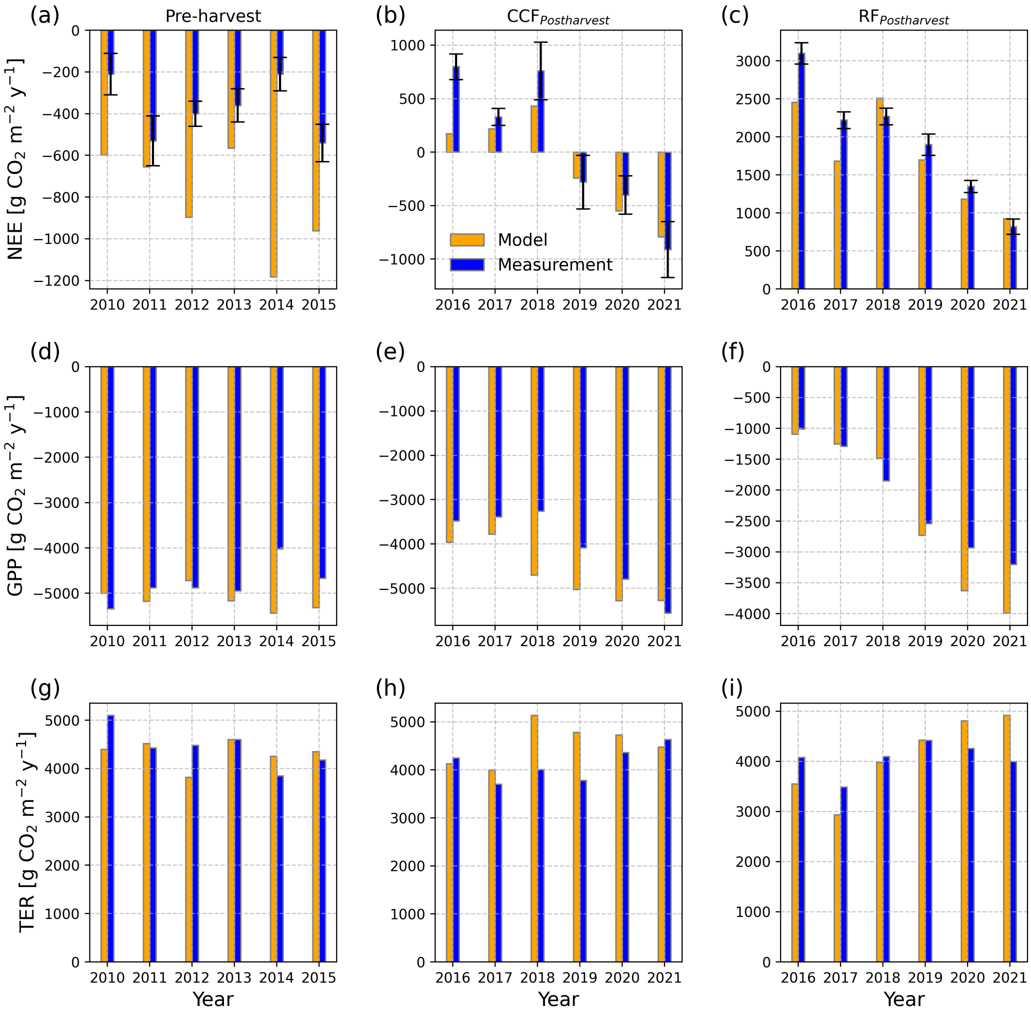

Figure 8. Annual balances of modeled net ecosystem exchange (NEE) and EC-based NEE (gapfilled) for pre-harvest, CCF$_{postharvest}$ and RF$_{postharvest}$ shown with the subplots **(a)**, **(b)** and **(c)**, respectively. Uncertainties in the EC-based NEE ~~(Korkiakoski et al., 2023)~~ calculated by Korkiakoski et al. (2023) following the uncertainty estimates by Heimsch et al. (2021) included statistical measurement error and gap-filling error. These uncertainties are shown with the error bars. ~~Similarly, pre-harvest~~Pre-harvest, CCF$_{postharvest}$ and RF$_{postharvest}$ gross primary product (GPP), are shown in **(d)**, **(e)** and **(f)** and total ecosystem respiration (TER), are shown in **(g)**, **(h)** and **(i)**, respectively. Negative values represent uptake by the ecosystem and positive values represent release of CO_2 to the atmosphere.

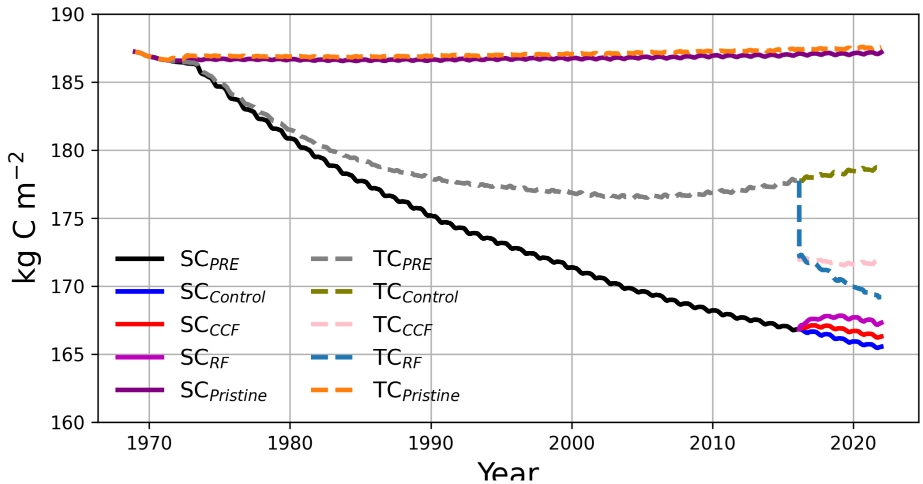

Figure 9. Modeled soil carbon (SC, solid lines) and total carbon (TC, dashed lines) time series for the different simulations from 1969 to 2021. Purple and orange show SC and TC for non-drained pristine peatland. Black and gray show the SC and TC development up to the harvest event in March 2016, respectively. Blue, red and magenta show the SC development for control, continuous cover forestry (CCF) and rotational forestry (RF) scenarios after harvest, respectively. Olive green, pink and light blue represent TC for control, CCF and RF scenarios after the harvest, respectively.

lated more carbon, and TC leveled off between 2000–2010 and showed an upward trend in ~~that time~~ later years as vegetation carbon uptake exceeded SC loss. In control, TC continued to increase until the end of the simulation. However, in CCF, TC decreased for a few years after the selective harvest and once the remaining vegetation rebounded TC started to increase again. In contrast, in RF, the accumulation of carbon by the forest stopped after the mature forest had been removed. Also, the newly planted forest was not accumulating enough carbon to offset the carbon lost from the soil, resulting in a downward trend in TC.

The litter pool (solutes) with a fast turnover rate had a high initial input from harvest, but the amount of solutes decreased very fast (Fig. ~~9a~~10a). After the initial spike, the solutes at RF were even lower than that of control and CCF in 2016-2019 since the remaining vegetation was not producing fresh litter. That rebounded once the birch started to influence the litter input from the fourth year after clear-cut. For both CCF and RF, after harvest, cellulose and lignin litter pools dominated the total litter pool, while solutes contributed comparatively little (Fig. ~~9b~~ 10b and c). Cellulose litter pool reached its peak in the third (RF) and second (CCF) year after the harvest and started to decrease after that, while the lignin litter pool started to decrease on the fourth year of harvest.

~~There was also an initial increase to the storage of fast decomposable labile humus poolafter the harvesting events~~ The bigger fraction of carbon in humus pools was allocated to the recalcitrant young pool (Fig. 10e) in the new version of model compared to older version (Fig. S15). Further, we saw the increase in heterotrophic respiration from older version to the newer version (Fig. S16) as a result of increased decomposition of larger recalcitrant young pool. After management, as a result of input from

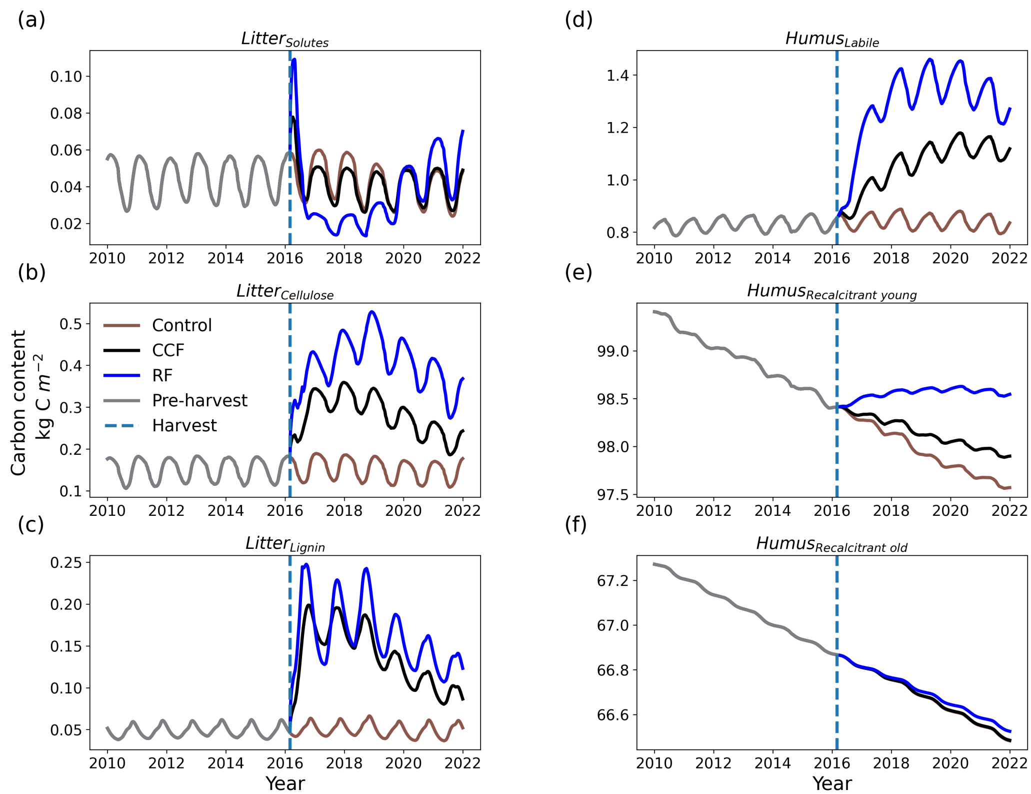

Figure 10. Litter (a, b and c) and humus (d, e and f) pools during pre-harvest and post-harvest conditions. Pre-harvest is shown in gray, control in brown, Continuous Cover Forestry (CCF) in black and Rotation Forestry (RF) in blue. Dashed light blue line shows the harvesting time.

freshly decomposed harvest residue, there was also an initial increase to the storage of fast decomposable labile humus pool (Fig. ~~9d). The peak in the labile storage was reached earlier in RF compared to CCF.~~ 10d). Contribution of decomposed harvest residue to the labile humus pool was larger in RF than CCF. The peak in the labile pool storage was reached earlier in RF compared to CCF. The decomposed harvest material also affected the recalcitrant young humus pool (Fig. ~~9e~~10e). A minimal effect on the recalcitrant old humus pool was seen after harvest from simulation (Fig. ~~9f~~10f).

4 Discussion

~~LDNDC model~~ The precess-based model LandscapeDNDC simulated the forest structure ~~realistically with the prescribed species composition for a~~ of the drained forested peatland realistically, both before and after the management events~~. Comparing~~

~~modeled LAI with~~, using the prescribed species composition. Simulated mature forest LAI was similar to the field estimated LAI reported by Leppä et al. (2020) ~~showed similar LAI values in a mature forest. But the sum of the modeled LAIs of all the~~ for the same site. Seasonal variation, the sum (2-4 m^2 / m^{-2}) of the three tree species (Pine, Spruce, and Birch) LAI in the simulation, was within the range reported by (Rautiainen et al., 2012) in several mixed forests in southern Finland. However, the summed modeled LAI of all individual tree species did not ~~gave the same perspective as satellite estimated LAI~~ correspond well with the satellite-estimated LAI for the site. This could be because the ~~satellite estimated~~ satellite-estimated LAI most likely reflects the ~~status of primary canopy of~~ primary canopy structure consisting of dominant pine and birch trees at the study site. ~~The~~ Indeed, the control stand had a dense canopy (Fig. A1) and the visibility of the secondary vegetation and forest floor can be poor with the satellite.

Modeled LAI matched with the satellite-estimated LAI well for CCF and RF stands after management because vegetation was sparse at the CCF stand immediately after selective harvest and almost no vegetation at the RF stand after clear-cut (Fig. A1). So model comparison with satellite estimate for these sparse vegetation stands gives much more accurate picture. Further, the declining trend in the modeled LAI for pine and spruce in control stand could be a result of competition between species in the model as well as the nutrient distribution among the species.

~~The model captured the temporal dynamics of the WT well and in the simulations the~~ While simulation using the site measured WT was possible with LDNDC, implementation of dynamic WT in this study gives the capability to generate the WT internally for peatland ecosystem. The fluctuations in WT, because of applied management, at the RF simulation were more pronounced ~~compared to the CCF, where~~ and captured by the model. However, the fluctuations were hard to distinguish in the CCF immediately after harvest, but simulated WT was similar to the measured WT already from the third year in CCF. Fluctuations in the WT due to management had been reported for the Lettosuo site from previous field studies (Leppä et al., 2020; Korkiakoski et al., 2019, 2020) and suggested an increase of 18-23 cm in WT at RF. ~~The simulated WT could not get below the prescribed Z_{gw} of 0.62m, which in turn have contributed to the trees not suffering from any drought effect in the simulations. As water was always available for the trees to uptake, this fact could explain why the effects of drought on CO_2 balance in summer 2018 (Korkiakoski et al., 2023) were not captured by the model when daily time series was investigated. But in annual scale for both CCF and RF the discrepancies in CO_2 balance in 2018 was not large even though 2018 was exceptionally dry (Lehtonen and Pirinen, 2019). This suggests that water availability below Z_{gw} for roots had only a minor influence in the overall CO_2 balance~~

The model was water-conserving in 2018, which could be related to the interaction between the vegetation and soil moisture. Saturated hydraulic conductivity and values used for VanGenuchten parameters, to calculate the water retention curve, might be restricting the water content from going below a certain level. However, thorough investigation of extreme drought episodes is out of the scope of this study as we focus on the general development of forests under different management regimes in typical climate conditions.

The simulation of the CH_4 fluxes for control and CCF was good, and the site was mostly a sink of CH_4. Simulation showed that the uptake in CCF stand, over the next five years after selective harvest, was on average 17% smaller than the control stand. Reduction in CH_4 uptake, after selective harvest, has been observed in drained peatland (Korkiakoski et al., 2020) as well as in an upland boreal forest (Sundqvist et al., 2014). Further, we investigated the autumn mismatch of CH_4 fluxes by changing the CH_4 oxidation and production parameters. While it shifted the CH_4 flux from higher sink to lower sink if CH_4 oxidation is low and vice versa, that did not remove the mismatch. We were satisfied with the simulated CH_4 flux, since it was within the observed CH_4 flux measured with chamber measurements. The chambers had different species abundance and that might impact how CH_4 was transported from soil to atmosphere within the chamber. Our model had simplistic ground vegetation and three tree species. Further, the individual chamber could have different soil moisture, water table, and soil temperature. Those might have an effect on the CH_4 flux. All these factors could result in the difference observed in the modeled CH_4 flux compared to the observed flux.

However, CH_4 flux dynamics after clear-cut in the RF were quite sensitive to the changes in WT. According to the measurements, RF changed from CH_4 sink to source after clear-cut (Korkiakoski et al., 2019). However, the model ~~was showing~~ showed the RF to be a sink of CH_4 after the clear-cut in the RF simulation with low WT, and a season-dependent source and sink in the RF simulation with high WT . Another measurement study with two different RF sites showed that the sites remained small sinks (0.07 and 0.52 mg CH_4 m^{-2} d^{-1}) of CH_4 even after clear-cut (Huttunen et al., 2003). CH_4 flux could be dependent on the localized WT . Thus, the placement of the chambers compared to the distance of ditches is an important factor to consider when comparing the model results with measurements (e.g., Laurén et al., 2021). The locations for the manual chambers in this study varied within 4–22.5 meters from the ditch and here we used an average WT from the chambers. Additionally, logger WTs were included in the study to cover the variability in the study site.

The simulated CO_2 annual balances showed net CO_2 sink similar to the observation for the pre-harvest period. Also, the simulated CO_2 annual balances for $CCF_{postharvest}$ and $RF_{postharvest}$ were in good agreement with the measurements in terms of when the stand (CCF) became a sink after harvest or how long the stand (RF) stayed a source.

In RF, after the clear-cut, the ecosystem was a source of CO_2 to the atmosphere according to both model and observations, which is largely due to the removed assimilation capacity of trees and increasing respiration from the harvest residuals (Korkiakoski et al., 2019). The underestimation in the NEE for first two years after clear-cut resulted from the model estimate of TER being lower compared to observations. The higher GPP in the year 2020 and 2021 is related to the introduction of the birch seedlings in 2019. The model only allows the seedlings to have a certain diameter (1 cm) at breast height and height of 50 cm when introduced for the first time. Thus, birch in the simulation may be slightly larger than the ones observed in the field conditions in 2020 and 2021, and resulted in higher GPP. Additionally, lower self-thinning could also result in the initial high GPP after birch reintroduction (Forrester et al., 2021). Thus, a lower number of seedlings than observed numbers can be used to get a more accurate GPP in the initial years. Indeed, a test with birch seedlings number of around 11000, instead of 17000, produced GPP values that were closer to the observation-based estimates.

In CCF, after selective harvest, the annual balance had a similar trend for both observation and simulation, where the first three years were a source of CO_2 and the next three years were a sink. However, we saw a small increase in the modeled GPP and TER already on the third year after the harvest, which was not evident in the observation-based GPP and TER. This could suggest that the simulation overestimates the recovery speed of the vegetation. ~~In RF, after the clear-cut, the ecosystem was a source of~~ The simulated WT could not get below the prescribed Z_{gw} of 0.62m, which in turn have contributed to the trees not suffering from any drought effect in the simulations. As water was always available for the trees to uptake, this fact could explain why the effects of drought on CO_2 balance in summer 2018 (Korkiakoski et al., 2023) were not captured by the model when daily time series was investigated. But on annual scale for both CCF and RF the discrepancies in CO_2 balance in 2018 was not large even though 2018 was exceptionally dry (Lehtonen and Pirinen, 2019). This suggests that water availability below Z_{gw} for roots had only a minor influence in the overall CO_2 ~~to the atmosphere according to both model and observations, which is largely due to the removed assimilation capacity of trees and increasing~~ balance.

Previously, the model was constructed to represent the mineral soil, thus changes to the carbon allocation in humus pools were necessary to capture the peatland characteristics. The soil layer with mineral soil allocation setup produced too low respiration from the ~~harvest residuals. Korkiakoski et al. (2019) reported the contribution from the harvest residue to the TER after clear-cut. The underestimation in the NEE for first two years after clear-cut resulted from the model estimate of TER being lower compared to observations~~soil. This was because, before modification to the pool allocation, a bigger fraction of carbon was allocated to the recalcitrant old pool. But with the new implementation a higher fraction of carbon was allocated to the recalcitrant young humus pool, which had a higher turnover rate than the recalcitrant old pool. Thus, it helped to increase the respiration associated with the decomposition of peat.

In this study the simulated annual soil carbon loss was -421 g C m^{-2} y^{-1} over 30-years period (1980-2009). A study by Simola et al. (2012), where 37 samples from peat sites with different fertility types from all over Finland were taken during the same time period, reported a minimum carbon loss from the drained peatland soil to be around -150 g C m^{-2} $year^{-1}$. Soil carbon loss at a fertile drained peatland site in southern Finland can even be around -1000 g C m^{-2} y^{-1} (Ojanen et al., 2013). Our study site is a MtkgII type peatland forest (Vasander and Laine, 2008). Different drained sites with the MtkgII status could have varying amounts of carbon loss from peat, which is regulated by WT and temperature (Ojanen et al., 2013). Thus the soil carbon loss from the simulation was in acceptable range when compared to the literature. The slowdown in SC loss for CCF and SC gain in RF compared to continuous SC loss in control was due to the large input of carbon from fresh litter and harvest residue into the soil. The residue contribution was larger in RF compared to CCF, resulting in the SC storage gaining more carbon in RF. Higher WT in the RF could also affect soil carbon storage, resulting in reduced carbon loss from soil. SC storage started to decrease again at the RF already from the fourth year after the harvest and for CCF even earlier as input from the decomposition of harvest residue started to diminish. Also the lowering of WT, because of the increased transpiration from the growing vegetation, started to contribute to the SC loss.

Overall, the model captured the transition of a mature forest stand to a forest stand that is under CCF and RF management. Annual CO_2 balances suggested the faster transition of a CCF stand from source to sink compared to RF stand, a result similar to observations (Korkiakoski et al., 2023). CH_4 sink was smaller in CCF compared to control stand and higher WT sensitivity for CH_4 flux was evident in RF. WT reacted faster in the RF compared to CCF after harvest but simulated WT for both were similar to the measurements in the later years after harvest.

The simulated LAI fluctuations in mature forest are likely related to species competition and nutrient distribution among species within the model and could be investigated further in future studies. The water conserving behavior of the model in drought years and associated CO_2 balance requires future considerations along with vegetation distributions within the chambers when comparing chamber measurements of CH_4. The simulations were run from the initial drainage year in 1969 to stand maturity to examine tree growth and soil carbon development over time. This long-term simulation approach was intended to ensure that the model can also be applied to future scenario analyses. Although the assessment of future scenarios is beyond the scope of this study, the model is well suited for investigating future developments of forest management practices, carbon dynamics, and water balance.

5 Conclusions

The process-based LandscapeDNDC model was successfully applied to simulate forest development under different managements on drained peatland from seedlings to maturity. The simulations demonstrated that estimates of carbon fluxes and the overall greenhouse gas balance vary substantially depending on management type, underscoring the importance of detailed information on management history, tree dimensions, and regrowth dynamics. The model reproduced measurement-derived NEE, GPP and TER both before and after harvest, while also capturing changes in forest structure. The implementation of a new dynamic water table (WT) module improved simulations of WT level, soil moisture, peat decomposition, and CH_4 fluxes, thereby enhancing the representation of carbon dynamics. We were able to illustrate the contributions of harvest residue to litter and humus pool and their decomposition. This successful application of LandscapeDNDC provides a robust basis for investigating future management scenarios in drained peatland forests, with respect to both carbon and energy balances. The model therefore offers valuable insights for developing forest management strategies that supports climate neutrality in peatland ecosystems.

Appendix A

A1 Lettosuo site

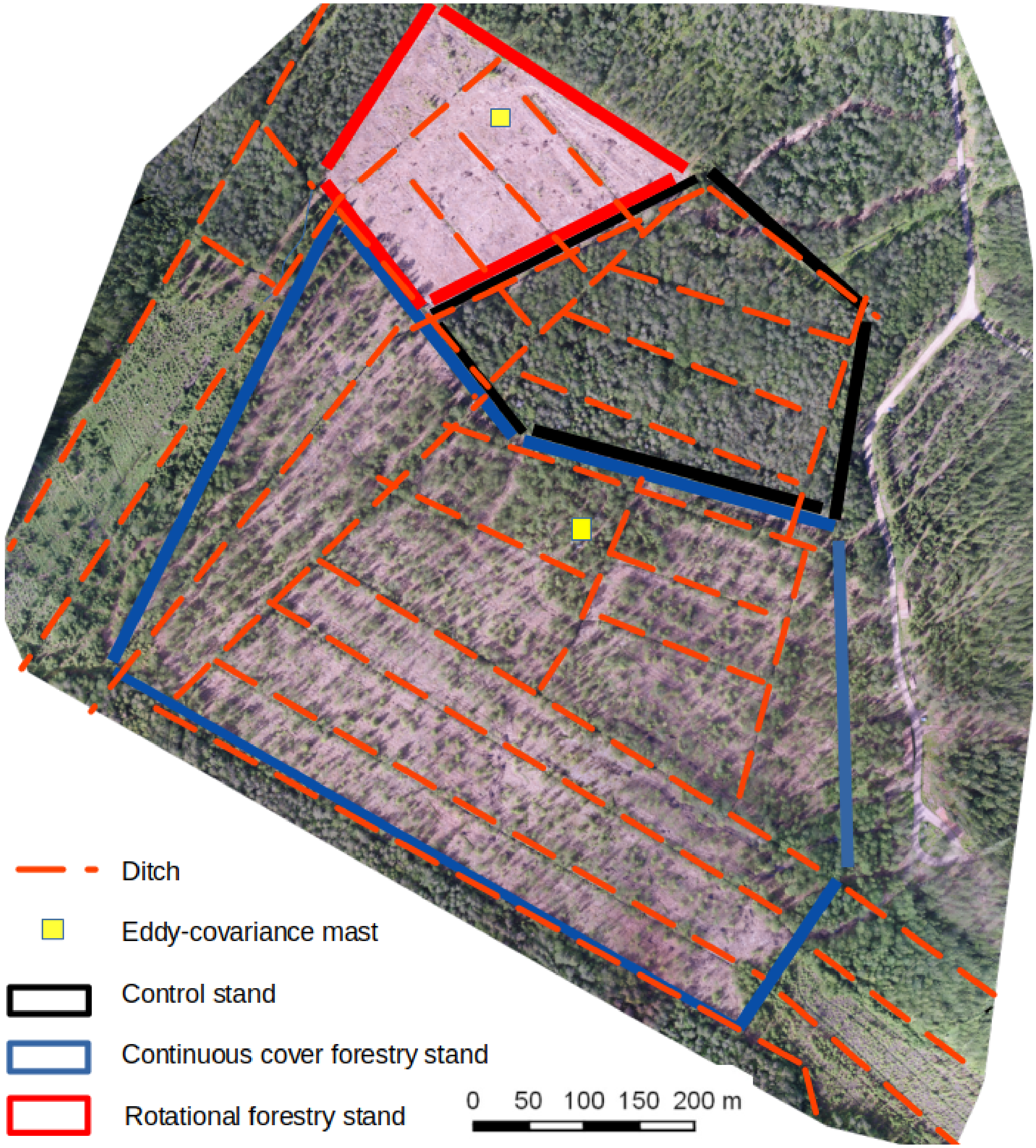

Figure A1. Aerial view of the Lettosuo site ~~.~~ taken on August 2016. Control, continuous cover forestry and rotational forestry stand are shown in black, blue and red boxes. Yellow squares mark the locations of the Eddy-covariance mast and orange dashed lines are showing the ditch network.

A2 Sensitivity test

Table A1: Sets of soil parameters (unitless) used in sensitivity test for soil processes (MeTr^x module).

Variable	Description	Range	Default	Best sensitivity test
Set 1				Best NSE_{NEE} 0.638
BETA LITTER TYPE	Exponential factor for litter decomposition reduction depending on lignin concentration	1 - 3	2	1.397
KR DC HUM1	Decomposition constant of labile humus	2×10^{-3} - 0.03	6.3×10^{-3}	7.55×10^{-3}
KR DC HUM2	Decomposition constant of recalcitrant young humus	5×10^{-5} - 3×10^{-3}	1.2×10^{-3}	6.34×10^{-4}
KR DC HUM3	Decomposition constant of recalcitrant old humus	1×10^{-6} - 1.25×10^{-4}	2.5×10^{-5}	2.6×10^{-5}
KR DC LIG	Decomposition constant of lignin	5×10^{-3} - 0.05	1.5×10^{-2}	1.39×10^{-2}
KR DC RAW LITTER	Decomposition constant of raw litter	5×10^{-3} - 0.1	0.02	8.58×10^{-2}
KR DC CEL	Decomposition constant of cellulose	1×10^{-4} - 0.01	2×10^{-3}	2.06×10^{-3}
KR DC SOL	Decomposition constant of solutes	0.1 - 0.8	0.4	0.24
KR DC WOOD	Decomposition constant of wood	5×10^{-5} - 1×10^{-3}	2.5×10^{-4}	2.39×10^{-4}
Set 2				Best NSE_{NEE} 0.641
KR REDUCTION ANVF	Decomposition reduction due anaerobicity	0.01 - 1.2	0.125	1.01
CO2 PROD DECOMP	Instantaneous production of CO2 during decomposition	0.1 - 0.6	0.3	0.52
KR REDUCTION CN	Decomposition reduction due to C:N ratio	1×10^{-3} - 0.01	5×10^{-3}	8.55×10^{-3}
F DECOMP T EXP1	Factor for temperature dependency of decomposition	0.5 - 5	3.5	4.28
F DECOMP T EXP2	Factor for temperature dependency of decomposition	25 - 45	35	41.8

Variable	Description	Range	Default	Best sensitivity test
F DECOMP PH1	Factor for pH dependency of decomposition	0.5 - 5	1.5	4.28
F DECOMP PH2	Factor for pH dependency of decomposition	0.1 - 5	3	1.04
F DECOMP M WEIBULL1	Factor for water filled pore space dependency of decomposition	0.1 - 0.9	0.595	0.76
F DECOMP M WEIBULL2	Factor for water filled pore space dependency of decomposition	5 - 15	8	13.40
Set 3				Best NSE_{NEE} 0.639
KR HU AORG HUM1	Rate constant for humification of active organic material to labile humus	5×10^{-4} - 0.1	1.5×10^{-2}	3.59×10^{-2}
KR HU AORG HUM2	Rate constant for humification of active organic material to recalcitrant young humus	1×10^{-5} - 0.01	6×10^{-3}	3.57×10^{-3}
KR HU CEL	Rate constant for humification of cellulose to labile humus	1×10^{-4} - 0.01	2×10^{-3}	3.63×10^{-3}
KR HU SOL	Rate constant for humification of solutes to labile humus	1×10^{-4} - 0.01	1×10^{-3}	3.64×10^{-3}
KR HU DOC	Rate constant for humification of dissolved carbon to labile humus	0 - 0.3	5×10^{-3}	0.10
KR HU HUM1	Rate constant for humification of labile humus to recalcitrant young humus	1×10^{-6} - 5×10^{-3}	7×10^{-5}	3.96×10^{-3}
KR HU HUM2	Rate constant for humification of recalcitrant young humus to recalcitrant old humus	1×10^{-7} - 5×10^{-4}	1×10^{-5}	1.79×10^{-4}
KR HU LIG	Rate constant for humification of lignin	1×10^{-3} - 0.1	1.5×10^{-2}	3.63×10^{-2}
METRX CN FRAC HUM3	C:N ratio fraction of humus 3 pool in relation to soil C:N ratio	0 - 1	0	0.36

Table A2: Species parameters used in running both the sensitivity tests and full forest runs. These remained constant unlike the soil parameters for sensitivity tests in Table A1.

Variable	Description	Adapted Value
	Forest floor	
DLEAFSHED	Total leaf longevity from the first day of emergence	300
GDDFOLSTART	Minimum temperature sum for foliage activity onset (°C)	0
KM20	Maintenance coefficient at reference temperature	1
VCMAX25	Maximum RubP saturated rate of carboxylation at 25°C for sun leaves ($\mu mol\ m^{-2}\ s^{-1}$)	66.8
SLAMAX	Specific leaf area in the shade ($m^2\ kg^{-1}$)	17 (*)
SLAMIN	Specific leaf area under full light ($m^2\ kg^{-1}$)	7 (*)
	Pine *(Pinus Sylvestris)*	
KM20	Maintenance coefficient at reference temperature	0.455
VCMAX25	Maximum RubP saturated rate of carboxylation at 25°C for sun leaves ($\mu mol\ m^{-2}\ s^{-1}$)	110.8
SLAMAX	Specific leaf area in the shade ($m^2\ kg^{-1}$)	15.1
SLAMIN	Specific leaf area under full light ($m^2\ kg^{-1}$)	3.4
	Spruce *(Picea Abies)*	
KM20	Maintenance coefficient at reference temperature	0.75
VCMAX25	Maximum RubP saturated rate of carboxylation at 25°C for sun leaves ($\mu mol\ m^{-2}\ s^{-1}$)	60.9
SLAMAX	Specific leaf area in the shade ($m^2\ kg^{-1}$)	8.3
SLAMIN	Specific leaf area under full light ($m^2\ kg^{-1}$)	3.8
	Birch *(Betula pendula/Pubescens)*	
DLEAFSHED	Total leaf longevity from the first day of emergence	300
GDDFOLSTART	Minimum temperature sum for foliage activity onset (°C)	111
KM20	Maintenance coefficient at reference temperature	0.07
VCMAX25	Maximum RubP saturated rate of carboxylation at 25°C for sun leaves ($\mu mol\ m^{-2}\ s^{-1}$)	38.4
SLAMAX	Specific leaf area in the shade ($m^2\ kg^{-1}$)	13
SLAMIN	Specific leaf area under full light ($m^2\ kg^{-1}$)	6.2

[*] 17 for pristine.

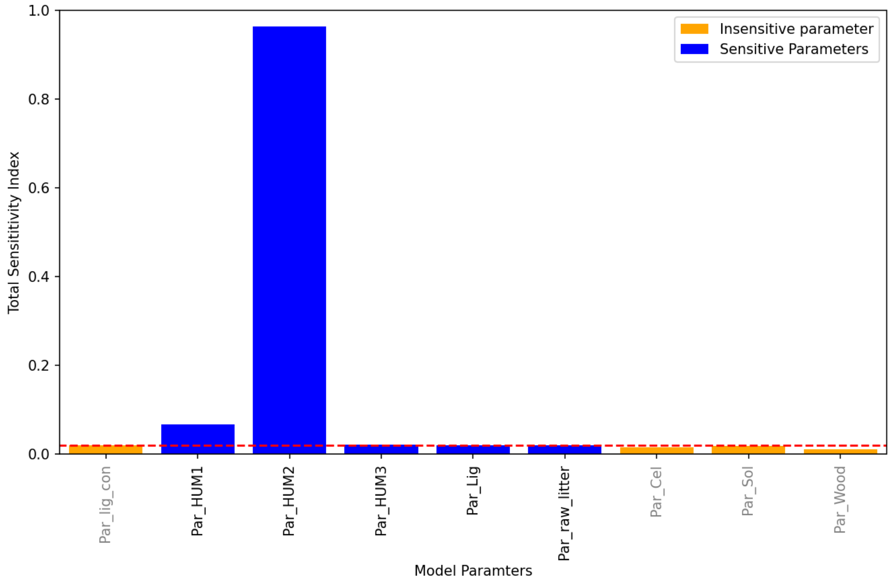

Figure A2. Sensitivity tests for the first set of parameters. Black x-ticks represents the five most sensitive parameters indicated by FAST algorithm and red dashed line indicate the threshold point in the Total sensitivity index for the fifth sensitive parameter. Threshold point for sensitive parameter is dependent on the user definition of number of sensitive parameter (e.g. in this case 5, but could have been any number between 1-9) in the algorithm. Grey x-ticks shows the non-sensitive parameters indicated by FAST.

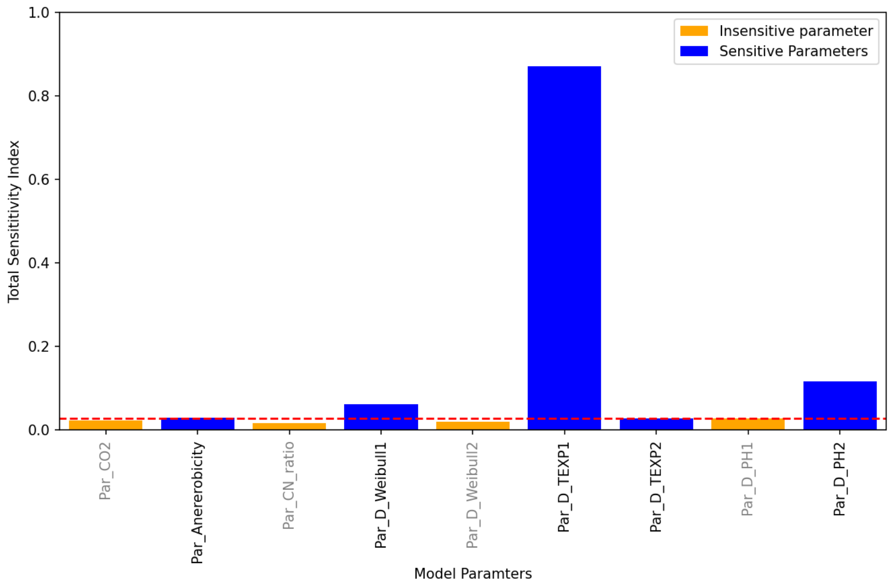

Figure A3. Sensitivity tests for the second set of parameters. Black x-ticks represents the five most sensitive parameters indicated by FAST algorithm and red dashed line indicate the threshold point in the Total sensitivity index for the fifth sensitive parameter. Grey x-ticks shows the non-sensitive parameters indicated by FAST.

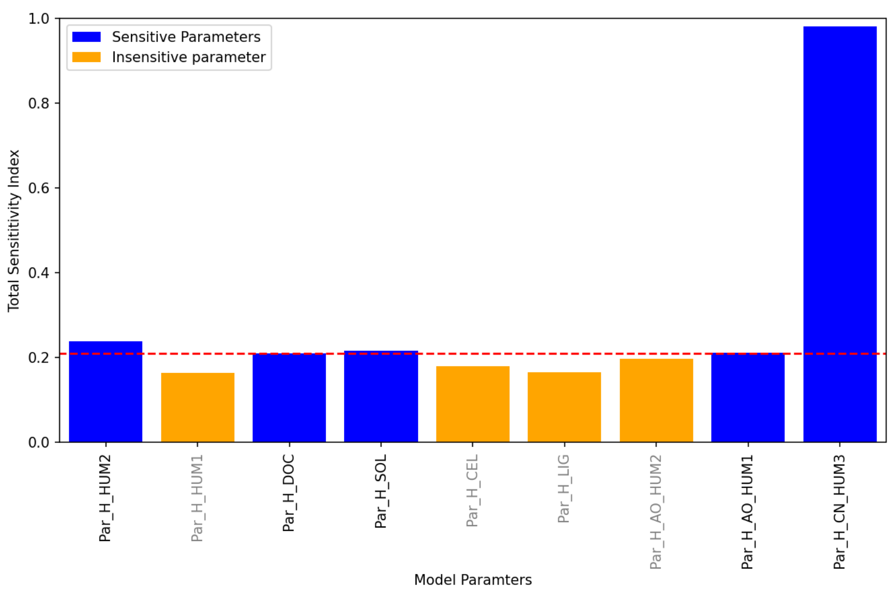

Figure A4. Sensitivity tests for the 3rd set of parameters. Black x-ticks represents the five most sensitive parameters indicated by FAST algorithm and red dashed line indicate the threshold point in the Total sensitivity index for the fifth sensitive parameter. Grey x-ticks shows the non-sensitive parameters indicated by FAST.

A3 ~~Parameters for~~ Full forest simulations

Table A3: Soil parameters (unitless unless stated) used in running the full forest simulations and their associated values.

Variable	Description	Adapted Value
CO2 PROD DECOMP	Instantaneous production of CO_2 during decomposition	0.35
F DECOMP T EXP 1	Factor for temperature dependency of decomposition	4
KR DC HUM 1	Decomposition constant of labile humus	0.03
KR DC HUM 2	Decomposition constant of recalcitrant young humus	3×10^{-3}
KR DC HUM 3	Decomposition constant of recalcitrant old humus	1.25×10^{-4}
KR DC RAW LITTER	Decomposition constant of raw litter	0.01
KR DC WOOD	Decomposition constant of wood	1×10^{-3}
KR FRAG ABOVE	Fragmentation constant of above-ground litter	0.01
KR FRAG BELOW	Fragmentation constant of below-ground litter	0.01
METRX MUEMAX C CH4 OX	Growth rate of methane oxidation microbes	0.60
METRX MUEMAX C CH4 PROD	Growth rate of methanogenic microbes	0.38
Ψ	Groundwater lateral gradient (m^{-1})	28.7 (38.7)

Code and data availability. Simulation and measurement data, python codes for analysis and codes for running SPOTPY are available https://doi.org/10.5281/zenodo.17397308, https://doi.org/10.5281/zenodo.18982316 and https://doi.org/10.5281/zenodo.20793091 (Shahriyer et al., 2025a, 2026a, b). Simulation setup can be found at https://doi.org/10.5281/zenodo.17987219 (Shahriyer et al., 2025b). Model source code can be found at https://doi.org/10.35097/8w3v0bf96c2xzenj. (Shahriyer et al., 2025c).

Author contributions. Model setup and running the simulations, data analysis, and writing of the article was done by AS with the support of TA, TM and DK. TA, TM, and AL conceptualized the study. Modifications to the model source code was done by DK and RG. MK and HR provided the measurement data, maintained the measurement systems and contributed to the text. Initial model setup, data analysis and reviewing of the text was done by SO, YG and HK. All coauthors contributed to the final reviews of the text.

Competing interests. The contact author has declared that none of the authors has any competing interests.

Acknowledgements. We are grateful for all the support that has enabled us to carry out the research. This project has received funding from the MMM Grant no. 4400T-2105 (TURNEE), and JTF-EP TUPSU. we are grateful for the support of the ACCC Flagship funded by the Research Council of Finland (grant no. 337552) and the Ministry of Transport and Communications through the Integrated Carbon Observation System (ICOS) and ICOS Finland (FIRI - ICOS Finland (345531)). This project further received funding from the European Union – NextGenerationEU instrument and was funded by the Research Council of Finland under grant no. 347794 (ForClimate), 324259 (BiBiFe), 341752 (RESPEAT), 374130 (PeatResC). Horizon Europe Framework Program of the European Union with grant no. 101056844 (Alfawetlands) and 101056848 (WETHORIZONS). D. Kraus received additional funding from the German Federal Ministry of Research, Technology and Space (BMFTR) project "Integrated Greenhouse Gas Monitoring System for Germany - Observations (ITMS-Q&S MODELPEAT) under grant number 01LK2305B. Minor modification to the text was done with the help of perplexity.ai.

References

Aalto, J., Pirinen, P., , and Jylhä, K.: New gridded daily climatology of Finland: Permutation-based uncertainty estimates and temporal trends in climate, J. Geophys. Res. Atmos, 121, 3807–3823, https://doi.org/10.1002/2015JD024651, 2016.

Baylay, S. E., Thormann, M. N., and Szumigalski, A. R.: Nitrogen mineralization and decomposition in western boreal bog and fen peat, Ecoscience, 12(4), 455–465, 2005.

Cade, S. M., Clemitshaw, K. C., Molina-Herrera, S., Grote, R., Haas, E., Wilkinson, M., Morison, J. I. L., and Yamulki, S.: Evaluation of LandscapeDNDC Model Predictions of CO_2 and N_2O Fluxes from an Oak Forest in SE England, Forests, 12,1517, https://doi.org/10.3390/f12111517, 2021.

Clarke, D. and Rieley, J.: Strategy for Responsible Peatland Management, International Peat Society, 2019.

Dirnböck, T., Kobler, J., Kraus, D., Grote, R., and Kiese, R.: Impacts of management and climate change on nitrate leaching in a forested karst area, Journal of Environmental Management, 165, 243–252, https://doi.org/10.1016/j.jenvman.2015.09.039, 2016.

Dirnböck, T., Kraus, D., Grote, R., Klatt, S., J.Kobler, Schindlbacher, A., Seidl, R., Thom, D., and Kies, R.: Substantial understory contribution to the C sink of a European temperate mountain forest landscape, Landscape Ecol, 35, 483–499, https://doi.org/10.1007/s10980-019-00960-2, 2020.

Findlay, S. E.: Chapter 4 - Organic Matter Decomposition, in: Fundamentals of Ecosystem Science (Second Edition), edited by Weathers, K. C., Strayer, D. L., and Likens, G. E., pp. 81–102, Academic Press, second edition edn., ISBN 978-0-12-812762-9, https://doi.org/https://doi.org/10.1016/B978-0-12-812762-9.00004-6, 2021.

Forrester, D. I., Baker, T. G., Hobi, S. R. E. M. L., Ouyang, S., Wiedemann, J. C., Xiang, W., Zell, J., and Pulkkinen, M.: Self-thinning tree mortality models that account for vertical stand structure, species mixing and climate, Forest Ecology and Management, 487, 118 936, 2021.

Grote, R., Mayrhofer, S., Fischbach, R., Steinbrecher, R., Staudt, M., and Schnitzler, J.-P.: Process-based modelling of isoprenoid emissions from evergreen leaves of Quercus ilex (L.), Atmospheric Environment, 40, S152–S165, https://doi.org/10.1016/j.atmosenv.2005.10.07, 2006.

Grote, R., Lavoir, A.-V., Rambal, S., Staudt, M., Zimmer, I., and Schnitzler, J.-P.: Modelling the drought impact on monoterpene fluxes from an evergreen Mediterranean forest canopy, Oecologia, 160, 213–223, https://doi.org/10.1007/s00442-009-1298-9, 2009.

Grote, R., Kiese, R., Grünwald, T., Ourcival, J.-M., and Granier, A.: Modelling forest carbon balances considering tree mortality and removal, Agricultural and Forest Meteorology, 151, 179–190, https://doi.org/10.1016/j.agrformet.2010.10.002, 2011.

Haas, E., Klatt, S., Fröhlich, A., Kraft, P., Werner, C., Kiese, R., Grote, R., Breuer, L., and Butterbach-Bahl, K.: LandscapeDNDC: a process model for simulation of biosphere–atmosphere–hydrosphere exchange processes at site and regional scale, Landscape Ecol, 28, 615–636, https://doi.org/10.1007/s10980-012-9772-x, 2013.

Haas, E., Carozzi, M., Massad, R. S., Butterbach-Bahl, K., and Scheer, C.: Long term impact of residue management on soil organic carbon stocks and nitrous oxide emissions from European croplands, Science of the Total Environment, 836 (2022) 154932, https://doi.org/10.1016/j.scitotenv.2022.154932, 2022.

Harmens, H., Norris, D., Cooper, D., Mills, G., Steinnes, E., Kubin, E., Thöni, L., Aboal, J., Alber, R., Carballeira, A., Coşkun, M., Temmerman, L. D., Frolova, M., González-Miqueo, L., Jeran, Z., Leblond, S., Liiv, S., Mankovská, B., Pesch, R., Poikolainen, J., Rühling, Å., Santamaria, J., Simonèiè, P., Schröder, W., Suchara, I., Yurukova, L., and Zechmeister, H.: Nitrogen concentrations in mosses indicate the spatial distribution of atmospheric nitrogen deposition in Europe, Environmental Pollution, 159, 2852–2860, https://doi.org/10.1016/j.envpol.2011.04.041, 2011.

He, H., Jansson, P.-E., M.Svensson, Björklund, J., Tarvainen, L., Klemedtsson, L., and Kasimir, Å.: Forests on drained agricultural peatland are potentially large sources of greenhouse gases – insights from a full rotation period simulation, Biogeosciences, 13, 2305–2318, https://doi.org/10.5194/bg-13-2305-2016, 2016.

Heimsch, L., Lohila, A., Tuovinen, J.-P., H. Vekuri, J. H., Nevalainen, O., Korkiakoski, M., Laurila, J. L. T., and Kulmala, L.: Carbon dioxide fluxes and carbon balance of an agricultural grassland in southern Finland, Biogeosciences, 18, 3467–3483, https://doi.org/10.5194/bg-18-3467-2021, 2021.

Houska, T., Kraft, P., Chamorro-Chavez, A., and Breuer, L.: SPOTting Model Parameters Using a Ready-Made Python Package, https://doi.org/10.1371/journal.pone.0145180, 2015.

Houska, T., Kraus, D., Kiese, R., and Breuer, L.: Constraining a complex biogeochemical model for multi-site greenhouse gas emission simulations by model-data fusion, Biogeosciences Discuss., https://doi.org/10.5194/bg-2017-96, 2017, 2017.

Huttunen, J. T., Nykänen, H., Martikainen, P. J., and Nieminen, M.: Fluxes of nitrous oxide and methane from drained peatlands following forest clear-felling in southern Finland, Plant and Soil, 255, 457–462, 2003.

Hytönen, J., Hökkä, H., and Saarinen, M.: The effect of planting, seeding and soil preparation on the regeneration success of Scots pine (Pinus sylvestris L.) on drained peatlands – 10-year results, Forestry Studies | Metsanduslikud Uurimused, 72, 91–106, https://doi.org/10.2478/fsmu-2020-0008, 2020.

Kasimir, Å., He, H., Coria, J., and Nordén, A.: Land use of drained peatlands: Greenhouse gas fluxes, plant production, and economics, Glob Change Biol, 24, 3302–3316, https://doi.org/10.1111/gcb.13931, 2018.

Korkiakoski, M., Tuovinen, J.-P., Aurela, M., Koskinen, M., Minkkinen, K., Ojanen, P., Penttilä, T., Rainne, J., Laurila, T., and Lohila, A.: Methane exchange at the peatland forest floor – automatic chamber system exposes the dynamics of small fluxes, Biogeosciences, 14, 1947–1967, 2017, 14, 1947–1967, 2017.

Korkiakoski, M., Tuovinen, J.-P., Penttilä, T., Sarkkola, S., Ojanen, P., Minkkinen, K., Rainne, J., Laurila, T., , and Lohila, A.: Greenhouse gas and energy fluxes in a boreal peatland forest after clear-cutting, Biogeosciences, 16, 3703–3723, 2019.

Korkiakoski, M., Ojanen, P., Penttilä, T., Minkkinen, K., Sarkkola, S., Rainne, J., Laurila, T., and Lohila, A.: Impact of partial harvest on CH4 and N2O balances of a drained boreal peatland forest, Agricultural and Forest Meteorology, 295 (2020) 108168, 2020.

Korkiakoski, M., Ojanen, P., Tuovinen, J.-P., Minkkinen, K., Nevalainen, O., Penttilä, T., Aurela, M., Laurila, T., and Lohila, A.: Partial cutting of a boreal nutrient-rich peatland forest causes radically less on-site CO2 emissions than clear-cutting, Agricultural and Forest Meteorology, 332 (2023) 109361, 2023.

Kraus, D., Weller, S., Klatt, S., Haas, E., Wassmann, R., Kiese, R., and Butterbach-Bahl, K.: A new LandscapeDNDC biogeochemical module to predict CH_4 and N_2O emissions from lowland rice and upland cropping systems, Plant Soil, 386, 125–149, https://doi.org/10.1007/s11104-014-2255-x, 2015.

Laiho, R.: Decomposition in peatlands: Reconciling seemingly contrasting results on the impacts of lowered water levels., Soil Biology and Biochemistry, 38(8), 2011–2024, 2006.

Laine, J.: Metsäojitettujen soiden luokittelu (Classification of forest drained peatlands), Suo, 40(1), 37–51, http://suo.fi/article/9651, 1989.

Laine, J., Silvola, J., Tolonen, K., Alm, J., Nykänen, H., Vasander, H., Sallantaus, T., Savolainen, I., Sinisalo, J., and Martikainen, P. J.: Effect of Water-Level Drawdown on Global Climatic Warming: Northern Peatlands, Ambio, 25, 179–184, 1996.

Laurén, A., Palviainen, M., Launiainen, S., Leppä, K., Stenberg, L., Urzainki, I., Nieminen, M., Laiho, R., and Hökkä, H.: Drainage and Stand Growth Response in Peatland Forests—Description, Testing, and Application of Mechanistic Peatland Simulator SUSI, Forests, 12,293, https://doi.org/10.3390/f12030293, 2021.

Lehtonen, I. and Pirinen, P.: 2018: An exceptionally dry thermal growing season in Finlands, FMI's Climate Bulletin: Research Letters, 1(1), 6, https://doi.org/10.35614/ISSN-2341-6408-IK-2019-04-RL, 2019.

Leppä, K., Korkiakoski, M., Nieminen, M., Laiho, R., Hotanen, J.-P., Kieloaho, A.-J., Korpela, L., Laurila, T., Lohila, A., Minkkinen, K., Mäkipää, R., Ojanen, P., Pearson, M., Penttilä, T., Tuovinen, J.-P., and Launiainen, S.: Vegetation controls of water and energy balance of a drained peatland forest: Responses to alternative harvesting practices, Agricultural and Forest Meteorology, 295 (2020) 108198, 2020.

Li, X., Markkanen, T., Korkiakoski, M., Lohila, A., Leppänen, A., Aalto, T., Peltoniemi, M., Mäkipää, R., Kleinen, T., and Raivonen, M.: Modelling alternative harvest effects on soil CO2 and CH4 fluxes from peatland forests, Science of Total Environment, 951, https://doi.org/10.1016/tj.scititenv.2024.175257, 2024.

Liu, C., Wang, Q., Mäkelä, A., Hökkä, H., Peltoniemi, M., and Hölttä, T.: A model bridging waterlogging, stomatal behavior and water use in trees in drained peatland, Tree physiology, 42, 1736–1749, https://doi.org/10.1093/trephys/tpac037, 2022.

Lohila, A., Laurila, T., Aro, L., Aurela, M., Tuovinen, J.-P., Laine, J., Kolari, P., and Minkkinen, K.: carbon dioxide exchange above a 30-year-old scots pine plantation established on organic-soil cropland, Boreal environment research, 12, 141–157, 2007.

Lohila, A., Minkkinen, K., Aurela, M., Tuovinen, J.-P., Penttilä, T., Ojanen, P., and Laurila, T.: Greenhouse gas flux measurements in a forestry-drained peatland indicate a large carbon sink, Biogeosciences, 8, 3203–3218, https://doi.org/10.5194/bg-8-3203-2011, 2011.

Makrickas, E., Manton, M., Angelstam, P., and Grygoruk, M.: Trading wood for water and carbon in peatland forests? Rewetting is worth more than wood production, Journal of Environmental Management, 341, 117 952, https://doi.org/10.1016/j.jenvman.2023.117952, 2023.

Meinshausen, M., Smith, S. J., Calvin, K., Daniel, J. S., Kainuma, M. L. T., Lamarque, J.-F., Matsumoto, K., Montzka, S. A., Raper, S. C. B., Riahi, K., Thomson, A., Velders, G. J. M., and van Vuuren, D. P. P.: The RCP greenhouse gas concentrations and their extensions from 1765 to 2300, Climatic Change, 109, 213–241, 2011.

Mezbahuddin, M., Grant, R. F., and Flanagan, L. B.: Coupled eco-hydrology and biogeochemistry algorithms enable the simulation of water table depth effects on boreal peatland net CO2 exchange, Biogeosciences, 14, 5507–5531, https://doi.org/10.5194/bg-14-5507-2017, 2017.

Minkkinen, K. and Laine, J.: Vegetation heterogeneity and ditches create spatial variability in methane fluxes from peatlands drained for forestr, Plant Soil, 285, 289–304, https://doi.org/10.1007/s11104-006-9016-4, 2006.

Minkkinen, K., Ojanen, P., Penttilä, T., Aurela, M., Laurila, T., Tuovinen, J.-P., and Lohila, A.: Persistent carbon sink at a boreal drained bog forest, Biogeosciences, 15, 3603–3624, https://doi.org/10.5194/bg-15-3603-2018, 2018.

Molina-Herrera, S., Grote, R., Santabárbara-Ruiz, I., Kraus, D., Klatt, S., Haas, E., Kiese, R., and Butterbach-Bahl, K.: Simulation of CO2 Fluxes in European Forest Ecosystems with the Coupled Soil-Vegetation Process Model "LandscapeDNDC", Forests, 6, 1779–1809, https://doi.org/10.3390/f6061779, 2015.

Mozafari, B., Bruen, M., Donohue, S., Renou-Wilson, F., and O'Loughlin, F.: Peatland dynamics: A review of process-based models and approaches, Science of the Total Environment, 877, https://doi.org/10.1016/j.scitotenv.2023.162890, 2023.

Nevalainen, O.: ollinevalainen/satellitetools: v1.0.0, a, https://doi.org/10.5281/ZENODO.5993292, 2022.

Nichols, J. E. and Peteet, D. M.: Rapid expansion of northern peatlands and doubled estimate of carbon storage, Nature Geoscience, 12, 917–921, https://doi.org/10.1038/s41561-019-0454-z, 2019.

Nieminen, M., Hökkä, H., Laiho, R., Juutinen, A., Ahtikoski, A., Pearson, M., Kojola, S., Sarkkola, S., Launiainen, S., Valkonen, S., Penttilä, T., Lohila, A., Saarinen, M., Haahti, K., Mäkipää, R., Miettinen, J., and Ollikainen, M.: Could continuous cover forestry be an economically and environmentally feasible management option on drained boreal peatlands?, Forest Ecology and Management, 424, 78–84, https://doi.org/10.1016/j.foreco.2018.04.046, 2018.

Ojanen, P., Minkkinen, K., and Penttilä, T.: The current greenhouse gas impact of forestry-drained boreal peatlands, Forest Ecology and Management, 289, 201–208, https://doi.org/10.1016/j.foreco.2012.10.008, 2013.

Quesada, G. D., Rautakoski, H., Xu, J., Li, Q., Larmola, T., Salovaara, P., Anttila, V., Peltoniemi, M., Koskinen, M., Lohila, A., Aalto, J., Lehtonen, A., Bäck, J., Mäkipää, R., Heinonsalo, J., Salmon, Y., and Lintunen, A.: Carbon dynamics after thinning in two boreal forest sites: Upland and drained peatland, Forest Ecology and Management, 595, https://doi.org/10.1016/j.foreco.2025.123024, 2026.

Rautiainen, M., Heiskanen, J., and Korhonen, L.: Seasonal changes in canopy leaf area index and MODIS vegetation products for a boreal forest site in central Finland, Boreal Environment Research, 17, 72–84, 2012.

Sarkkola, S., Hökkä, H., Koivusalo, H., Nieminen, M., Ahti, E., Päivänen, J., and Laine, J.: Role of tree stand evapotranspiration in maintaining satisfactory drainage conditions in drained peatlands, Canadian Journal of Forest Research, 40, https://doi.org/10.1139/X10-084, 2010.

Shahriyer, A. H., Kraus, D., Markkanen, T., Korkiakoski, M., Rautakoski, H., Orttenvuori, S., Gao, Y., Kajasilta, H., Grote, R., Lohila, A., and Aalto, T.: Dataset and python codes: Evaluation of the LandscapeDNDC model for drained peatland forest managements, LDNDC v1.35.2 (revision 11434), https://doi.org/10.5281/zenodo.17397308, 2025a.

Shahriyer, A. H., Kraus, D., Markkanen, T., Korkiakoski, M., Rautakoski, H., Orttenvuori, S., Gao, Y., Kajasilta, H., Grote, R., Lohila, A., and Aalto, T.: Simulation setup: Evaluation of the LandscapeDNDC model for drained peatland forest managements, LDNDC v1.35.2 (revision 11434), https://doi.org/10.5281/zenodo.17987219, 2025b.

Shahriyer, A. H., Kraus, D., Markkanen, T., Korkiakoski, M., Rautakoski, H., Orttenvuori, S., Gao, Y., Kajasilta, H., Grote, R., Lohila, A., and Aalto, T.: Simulation model code: Evaluation of the LandscapeDNDC model for drained peatland forest managements, LDNDC v1.35.2 (revision 11434), https://doi.org/10.35097/8w3v0bf96c2xzenj, 2025c.

Shahriyer, A. H., Kraus, D., Markkanen, T., Korkiakoski, M., Rautakoski, H., Orttenvuori, S., Gao, Y., Kajasilta, H., Grote, R., Lohila, A., and Aalto, T.: Dataset and python codes: Evaluation of the LandscapeDNDC model for drained peatland forest managements, LDNDC v1.35.2 (revision 11434), https://doi.org/10.5281/zenodo.18982316, 2026a.

Shahriyer, A. H., Kraus, D., Markkanen, T., Korkiakoski, M., Rautakoski, H., Orttenvuori, S., Gao, Y., Kajasilta, H., Grote, R., Lohila, A., and Aalto, T.: Dataset and python codes: Evaluation of the LandscapeDNDC model for drained peatland forest managements, LDNDC v1.35.2 (revision 11434), https://doi.org/10.5281/zenodo.20793091, 2026b.

Shi, X., Ricciuto, D. M., Thornton, P. E., Xu, X., Yuan, F., Norby, R. J., Walker, A. P., Warren, J. M., Mao, J., Hanson, P. J., Meng, L., Weston, D., and Griffiths, N. A.: Extending a land-surface model with Sphagnum moss to simulate responses of a northern temperate bog to whole ecosystem warming and elevated CO2, Biogeosciences, 18, 467–486, https://doi.org/10.5194/bg-18-467-2021, 2021.

Silva, M. P., Healy, M. G., and Gill, L.: Reviews and syntheses: A scoping review evaluating the potential application of ecohydrological models for northern peatland restoration, Biogeosciences, 21, 3143–3163, https://doi.org/10.5194/bg-21-3143-2024, 2024.

Simola, H., Pitkänen, A., and Turunen, J.: Carbon loss in drained forestry peatlands in Finland, estimated by re-sampling peatlands surveyed in the 1980s, European Journal of Soil Science, https://doi.org/10.1111/j.1365-2389.2012.01499.x, 2012.

Sundqvist, E., Vestin, P., Crill, P., Persson, T., and Lindroth, A.: Short-term effects of thinning, clear-cutting and stump harvesting on methane exchange in a boreal forest., Biogeosciences, 11, 6095–6105, https://doi.org/10.5194/bg-11-6095-2014, 2014.

Tong, C. H. M., Noumonvi, K. D., Ratcliffe, J., Laudon, H., Järveoja, J., Drott, A., Nilsson, M. B., and Peichl, M.: A drained nutrient-poor peatland forest in boreal Sweden constitutes a net carbon sink after integrating terrestrial and aquatic fluxes, Global Change Biology, 30, e17 246, https://doi.org/10.1111/gcb.17246, 2024.

Turunen, J. and Valpola, S.: The influence of anthropogenic land use on Finnish peatland area and carbon stores 1950–2015, Mires and Peat, 26, https://doi.org/10.19189/MaP.2019.GDC.StA.1870, 2020.

Vasander, H. and Laine, J.: Site type classification on drained peatlands, Korhonen, R., Korpela, L., Sarkkola, S. (Eds.). Finland – Fenland: Research and Sustainable Utilisation of Mires and Peat. Finnish Peatland Society, Maahenki Ltd., Helsinki, pp. 146–151, 2008.

Werner, C., Haas, E., Grote, R., Gauder, M., Graeff-Hönninger, S., Claupein, W., and Butterbach-Bahl, K.: Biomass production potential from Populus short rotation systems in Romania, GCB Bioenergy, 4, no 6, 642–653, https://doi.org/10.1111/j.1757-1707.2012.01180.x, 2012.